Table 3. Genes up-regulated in $CD4^+$ T cells from cord blood samples 1 and 2 (CB 1 and CB 2, respectively)

		Fold change				
Affi ID	Gene abbreviation	CB 1	CB 2	PB 1	PB 2	Gene name
Apoptosis						
1555372_at	*BimL*	1·39	1·52	0·61	0·42	BCL2-like 11 (apoptosis facilitator)
237837_at	*BCL2*	1·27	1·32	0·49	0·73	B-cell CLL/lymphoma 2
205681_at	*BCL2A1*	1·91	1·53	0·39	0·47	BCL2-related protein A1
1558143_a_at	*BCL2L11*	1·68	1·74	0·32	0·32	BGL2-like 11 (apoptosis facilitator)
228311_at	*BCL6B*	1·36	3·39	0·64	0·26	B-cell CLL/lymphoma 6, member B (zinc finger protein)
215037_s_at	*BCLX*	2·56	1·27	0·73	0·56	BCL2-like 1
224414_s_at	*CARD6*	2·65	1·34	0·56	0·66	Caspase recruitment domain family, member 6
201631_s_at	*IER3*	1·62	2·95	0·38	0·31	Immediate early response 3
218000_s_at	*PHLDA1*	2·34	1·21	0·53	0·79	Pleckstrin homology-like domain, family A, member 1
209803_s_at	*PHLDA2*	2·87	1·32	0·31	0·68	Pleckstrin homology-like domain, family A. member 2
203063_at	*PPMIF*	1·26	1·53	0·74	0·64	Protein phosphatase IF (PP2C domain containing)
205214_at	*STK17B*	1·78	1·26	0·74	0·71	Serine/threonine kinase 17b (apoptosis-inducing)
217853_at	*TENS1*	1·63	6·00	0·04	0·37	Tensin 1
B- and T-cell development						
211861_x_at	*CD28*	1·35	1·41	0·49	0·65	CD28 antigen(Tp44)
207892_at	*CD40LG*	3·67	1·32	0·45	0·68	C040 ligand (TNF superfamily, member 5, hyper-IgM syndrome)
206914_at	*CRTAM*	2·76	1·60	0·40	0·36	Class I MHC-restricted T-cell-associated molecule
210557_x_at	*CSF1*	3·79	1·22	0·78	0·70	Colony-stimulating factor 1 (macrophage)
210229_s_at	*CSF2*	1·28	2·67	0·69	0·72	Colony-stimulating factor 2 (granulocyte–macrophage)
205159_at	*CSF2RB*	2·33	1·60	0·18	0·40	Colony-stimulating factor 2 receptor
231794_at	*CTLA4*	1·39	1·26	0·74	0·44	Cytotoxic T-lymphocyte-associated protein 4
204232_at	*FCER1G*	1·63	2·14	0·28	0·37	Fc fragment of IgE, high affinity 1, receptor for; gamma polypeptide
210439_at	*ICOS*	1·38	1·34	0·57	0·66	Inducible T-cell costimulator
210354_at	*IFNG*	1·48	1·92	0·46	0·52	Human mRNA for HuIFN -gamma interferon
230536_at	*PBX4*	1·48	1·26	0·50	0·74	Pre-B-cell leukaemia transcription factor 4
215540_at	*TCRA*	1·25	1·87	0·67	0·75	T-cell antigen receptor alpha
234440_al	*TCRD*	7·51	1·48	0·50	0·52	Human T-cell receptor delta-chain
Cell growth and maintenance						
213497_at	*ABTB2*	2·06	1·34	0·66	0·63	Ankyrin repeat and BTB (POZ) domain containing 2
201236_s_at	*BTG2*	1·60	1·23	0·60	0·77	BTG family, member 2
235287_at	*CDK6*	1·50	1·32	0·44	0·68	Cyclin-dependent kinase 6
209644_x_at	*CDKN2A*	2·90	1·21	0·67	0·79	Cyclin-dependent kinase inhibitor 2A (melanoma, p16, inhibits CDK4)
236313_at	*CDKN2B*	3·24	1·28	0·58	0·72	Cyclin-dependent kinase inhibitor 2B (p15, inhibits CDK4)
241984_at	*CHES1*	1·38	1·34	0·66	0·63	Checkpoint suppressor 1
202552_s_at	CRIM1	1·94	1·39	0·32	0·61	Cysteine-rich transmembrane BMP regulator 1 (chordin-like)
204844_at	*ENPEP*	1·64	1·75	0·09	0·36	Glutamyl aminopeptidase (aminopeptidase A)
205418_at	*FES*	1·39	1·80	0·61	0·25	Feline sarcoma oncogene
228572_at	*GRB2*	4·69	1·21	0·79	0·78	Growth factor receptor-bound protein 2
207688_s_at	*INHBC*	1·46	1·25	0·51	0·75	Inhibin, beta C
209744_x_at	*ITCH*	1·30	1·47	0·63	0·70	Itchy homolog E3 ubiquitin protein ligase (mouse)
201548_s_at	*JARID1B*	1·27	1·92	0·73	0·46	Jumonji, AT-rich interactive domain IB (RBP2-like)
203297_s_at	*JARID2*	1·42	1·28	0·54	0·72	Jumonji, AT-rich interactive domain 2
41387_r_at	*JMJD3*	1·82	1·24	0·76	0·65	Jumonji domain containing 3
205569_at	*LAMP3*	2·32	1·24	0·76	0·50	Lysosomal-associated membrane protein 3
214039_s_at	*LAPTM4B*	1·41	1·49	0·49	0·59	Lysosomal-associated protein transmembrane 4 beta
205857_x_at	*MSH3*	1·79	1·28	0·58	0·72	MutS homolog 3 (*E. coli*)
209550_at	*NDN*	3·42	1·38	0·17	0·62	Necdin homolog (mouse)
207943_x_at	*PLAGL1*	1·37	1·43	0·57	0·63	Pleiomorphic adenoma gene-like 1
204748_at	*PTGS2*	1·65	1·78	0·14	0·35	Prostaglandin-endoperoxide synthase 2
201482_at	*QSCN6*	1·32	1·23	0·38	0·77	Quiescin Q6
203743_s_at	*TDG*	1·47	1·23	0·54	0·77	Thymine-DNA glycosylase
204227_s_at	*TK2*	2·12	1·26	0·56	0·74	Thymidine kinase 2, mitochondrial

Table 3. Continued

Affi ID	Gene abbreviation	Fold change CB 1	CB 2	PB 1	PB 2	Gene name
Cytokines and chemokines						
207533_at	*CCL1*	1·67	1·48	0·52	0·49	Chemokine (C-C motif) ligand 1
205099_s_at	*CCR1*	4·70	1·21	0·61	0·79	Chemokine (C-C motif) receptor 1
207681_at	*CXCR3*	1·51	1·33	0·41	0·67	Chemokine (C-X-C motif) receptor 3
211469_s_at	*CXCR6*	1·58	1·95	0·32	0·42	Chemokine (C-X-C motif) receptor 6
206613_at	*IL-18R1*	2·32	1·38	0·61	0·62	Interleukin-18 receptor 1
207072_at	*IL-18RAP*	2·16	1·44	0·46	0·56	Interleukin-18 receptor accessory protein
212657_s_at	*IL-1RN*	1·44	3·12	0·56	0·37	Interleukin 1 receptor
206341_at	*IL-2RA*	1·52	1·27	0·73	0·66	Interleukin-2 receptor alpha
202859_x_at	*IL-8*	1·31	3·75	0·38	0·69	Interleukin-8
202643_s_at	*TNFAIP3*	1·61	1·25	0·67	0·75	Tumour necrosis factor, alpha-induced protein 3
202687_s_at	*TNFSF10*	2·83	1·23	0·67	0·77	Tumour necrosis factor (ligand) superfamily member 10
205599_at	*TRAF1*	2·25	1·32	0·68	0·61	Tumour necrosis factor receptor-associated factor 1
202871_at	*TRAF4*	1·43	1·58	0·57	0·48	Tumour necrosis factor receptor-associated factor 4
206366_x_at	*XCL1*	1·24	2·66	0·46	0·76	Chemokine (C motif) ligand 1
Signal transduction						
210538_s_at	*AIP1*	1·35	1·54	0·65	0·61	Baculoviral IAP repeat-containing 3
209369_at	*ANXA3*	1·39	6·82	0·61	0·05	Annexin A3
1554343_a_at	*BRDG1*	1·45	1·67	0·52	0·55	BCR downstream signalling 1
225946_at	*C12orf2*	3·20	1·77	0·23	0·23	Ras association (RaIGDS/AF-6) domain family 8
204392_at	*CAMK1*	1·26	1·62	0·74	0·54	Calcium/calmodulin-dependent protein kinase I
231042_s_at	*CAMK2D*	1·31	1·63	0·25	0·69	Calcium/calmodulin-dependent protein kinase (CaM kinase) II delta
205692_s_at	*CD38*	1·37	1·29	0·71	0·48	CD38 antigen (p45)
231747_at	*CYSLTR1*	3·16	1·45	0·55	0·43	Cysteinyl leukotriene receptor 1
211272_s_at	*DGKA*	1·43	1·23	0·77	0·54	Diacylglycerol kinase alpha 80 kDa
200762_at	*DPYSL2*	1·35	1·40	0·37	0·65	Dihydropyrimtdinase-like 2
208370_s_at	*DSCR1*	1·23	1·90	0·63	0·77	Down syndrome critical region gene 1
204794_at	*DUSP2*	1·55	2·57	0·39	0·45	Dual specificity phosphatase 2
204015_s_at	*DUSP4*	1·35	2·66	0·65	0·39	Dual specificity phosphatase 4
211333_s_at	*FASLG*	1·20	1·37	0·49	0·80	Fas ligand (TNF superfamily, member 6)
211535_s_at	*FGFR1*	1·23	2·79	0·70	0·77	Fibroblast growth factor receptor 1
224148_at	*FYB*	1·50	1·21	0·45	0·79	FYN binding protein (FYB-120/130)
209304_x_at	*GADD45B*	1·55	1·29	0·65	0·71	Growth arrest and DNA-damage-inducible beta
234284_at	*GNG8*	1·50	3·16	0·50	0·35	Guanine nucleotide binding protein (G protein), gamma 8
224285_at	*GPR174*	1·91	1·42	0·56	0·58	G protein-coupled receptor 174
223767_at	*GPR84*	4·41	1·44	0·05	0·56	G protein-coupled receptor 84
211555_s_at	*GUCY1B3*	1·66	1·73	0·34	0·03	Guanylate cyclase 1, soluble, beta 3
38037_at	*HBEGF*	1·54	1·36	0·55	0·64	Heparin-binding EGF-like growth factor
203820_s_at	*IMP-3*	1·83	2·18	0·17	0·17	IGF-II-mRNA-binding protein 3
203006_at	*INPP5A*	1·40	1·86	0·60	0·52	Inositol polyphosphate-5-phosphatase, 40 kDa
231779_at	*IRAK2*	1·93	1·46	0·46	0·54	Interleukin-1 receptor associated kinase 2
32137_at	*JAG2*	1·58	1·29	0·71	0·64	Jagged 2
203904_x_at	*KAI1*	1·65	1·59	0·41	0·25	CD82 antigen
235252_at	*KSR*	1·72	1·56	0·43	0·44	Kinase suppressor of ras 1
210948_s_at	*LEF1*	1·21	1·64	0·41	0·79	Hypothetical protein LOC641518
203236_s_at	*LGALS9*	1·48	1·27	0·73	0·51	Lectin, galactoside-binding, soluble, 9 (galectin 9)
220253_s_at	*LRP12*	1·27	1·30	0·31	0·73	Low-density lipoprotein-related protein 12
206637_at	*P2RY14*	1·32	1·48	0·39	0·68	Purinergic receptor P2Y, G-protein coupled, 14
210837_s_at	*PDE4D*	1·35	1·31	0·62	0·69	Phosphodiesterase 4D, cAMP-specific
206726_at	*PGDS*	6·45	1·40	0·60	0·43	Prostaglandin D2 synthase, haematopoietic
210617_at	*PHEX*	1·53	4·08	0·21	0·47	Phosphate regulating endopeptidase homologue, X-linked
206370_at	*PIK3CG*	1·23	1·32	0·50	0·77	Phosphoinositide-3-kinase, catalytic, gamma polypeptide
205632_s_at	*PIP5K1B*	1·32	1·42	0·64	0·68	Phosphalidylinositol-4-phosphate 5-kinase, type 1 beta

Table 3. Continued

Affi ID	Gene abbreviation	Fold change CB 1	CB 2	PB 1	PB 2	Gene name
215195_at	*PRKCA*	2·17	1·36	0·64	0·61	Protein kinase C, alpha
210832_x_at	*PTGER3*	4·44	1·47	0·07	0·53	Prostaglandin E receptor 3 (subtype EP3)
1553535_a_at	*RANGAP1*	1·58	1·39	0·58	0·61	Ran GTPase activating protein 1
234344_at	*RAP2C*	1·75	1·26	0·46	0·74	RAP2C, member of RAS oncogene family
223809_at	*RGS18*	2·12	1·67	0·15	0·33	Regulator of G-protein signalling 18
209882_at	*RIT1*	1·74	1·32	0·63	0·68	Ras-like without CAAX 1
209451_at	*TANK*	1·34	1·20	0·42	0·80	TRAF family member-associated NFKB activator
204924_at	*TLR2*	1·60	2·52	0·36	0·40	Toll-like receptor 2
217979_at	*TM4SF13*	1·21	2·47	0·30	0·79	Tetraspanin 13
209263_x_at	*TM4SF7*	2·05	1·41	0·58	0·59	Tetraspanin 4
Transcription						
1566989_at	*ARID1B*	1·42	1·27	0·09	0·73	AT-rich interactive domain 1B (SWIl-like)
203973_s_at	*CEBPD*	3·06	1·51	0·33	0·49	CCAAT/enhancer binding protein (C/EBP), delta
221598_s_at	*CRSP8*	1·60	1·29	0·71	0·68	Cofactor required for Spl transcriptional activation, subunit 8, 34 kDa
205249_at	*EGR2*	1·33	4·27	0·67	0·60	Early growth response 2 (Krox-20 homologue, *Drosophila*)
206115_at	*EGR3*	1·31	6·15	0·69	0·48	Early growth response 3
201328_at	*ETS2*	1·57	1·72	0·43	0·40	V-ets erythroblastosis virus E26 oncogene homologue 2 (avian)
218810_at	*FLJ23231*	2·13	1·37	0·63	0·63	Zinc finger CCCH-type containing 12A
209189_at	*FOS*	21·56	1·31	0·13	0·69	V-fos FBJ murine osteosarcoma viral oncogene homologue
223408_s_at	*FOXK2*	2·26	1·22	0·48	0·78	Forkhead box K2
202723_s_at	*FOXO1A*	1·47	1·27	0·57	0·73	Forkhead box O1A (rhabdomyosarcoma)
224211_at	*FOXP3*	1·62	1·41	0·59	0·23	Forkhead box P3
207156_at	*HIST1H2AG*	1·73	1·30	0·41	0·70	Histone 1, H2ag
220042_x_at	*HIVEP3*	1·26	1·65	0·74	0·56	Human immunodeficiency virus type I enhancer binding protein 3
207826_s_at	*ID3*	1·34	8·64	0·60	0·66	Inhibitor of DNA binding 3, dominant negative helix-loop-hetix protein
204549_at	*IKBKE*	2·33	1·29	0·71	0·66	Inhibitor of kappa light polypeptide gene enhancer in B cells
219878_s_at	*KLF13*	1·89	1·26	0·34	0·74	Kruppel-like factor 13
207667_s_at	*MAP2K3*	1·33	1·28	0·72	0·57	Mitogen-activated protein kinase kinase 3
201502_s_at	*NFKBIA*	2·31	1·29	0·71	0·57	Nuclear factor of κ light polypeptide gene enhancer in B cells inhibitor
222105_s_at	*NKIRAS2*	1·84	1·21	0·69	0·79	NFKB inhibitor interacting Ras-like 2
204622_x_at	*NR4A2*	1·35	4·31	0·65	0·63	Nuclear receptor subfamily 4, group A, member 2
207978_s_at	*NR4A3*	1·33	3·53	0·62	0·67	Nuclear receptor subfamily 4, group A, member 3
202600_s_at	*NRIPI*	1·86	1·39	0·26	0·61	Nuclear receptor interacting protein 1
216841_s_at	*SOD2*	1·25	1·73	0·36	0·75	Superoxide dismutase 2, mitochondrial
201416_at	*SOX4*	1·53	2·21	0·47	0·38	SRY (sex determining region Y)-box 4
223635_s_at	*SSBP3*	2·12	1·25	0·75	0·62	Single-stranded DNA binding protein 3
206506_s_at	*SUPT3H*	1·47	1·31	0·57	0·69	Suppressor of Ty 3 homologue (*S. cerevisiae*)
221618_s_at	*TAF9L*	1·25	1·49	0·47	0·75	TAF9-like RNA polymerase II
203177_x_at	*TFAM*	1·63	1·23	0·77	0·57	Transcription factor A, mitochondrial
213943_at	*TWIST1*	1·89	3·14	0·04	0·11	Twist homologue 1 (acrocephalosyndactyly 3; Saethre-Chotzen syndrome)
219836_at	*ZBED2*	1·33	4·76	0·67	0·21	Zinc finger, BED-type containing 2
211965_at	*ZFP36L1*	2·02	1·47	0·29	0·53	Zinc finger protein 36, C3H type-like 1
230760_at	*ZFY*	1·41	1·25	0·75	0·02	Zinc finger protein, Y-linked
228854_at	*ZNF145*	3·26	1·21	0·40	0·79	Transcribed locus
235121_at	*ZNF542*	2·68	1·33	0·63	0·67	Zinc finger protein 542

To investigate whether increased expression of the *IL-17* gene is a general feature of PB-derived $CD4^+$ T cells, we also tested *IL-17* gene expression in the above-described additional samples by real-time RT-PCR analysis. As shown in Fig. 6, all of four PB-derived $CD4^+$ T-cell samples revealed significantly increased gene expression of *IL-17* when compared with the CB-derived samples at 1 week. At 2 weeks, however, *IL-17* gene expression in PB-derived $CD4^+$ T cells was diminished while some of the CB-derived $CD4^+$ T cells (such as sample CB 4) exhibited increased *IL-17* gene expression. When the data were analysed statistically, expression of the *IL-17* gene was found to be

Table 4. Genes up-regulated in $CD4^+$ T cells from peripheral blood (PB)

Affi ID	Gene abbreviation	Fold change CB 1	CB 2	PB 1	PB 2	Gene name
Apoptosis						
1553681_a_at	*PRF1*	0·66	0·51	1·41	1·34	Perforin 1 (pore-forming protein)
B- and T-cell development						
224499_s_at	*AICDA*	0·06	0·44	1·56	3·47	Activation-induced cytidine deaminase
205495_s_at	*GNLY*	0·40	0·51	1·49	6·34	Granulysin
217478_s_at	*HLA-DMA*	0·67	0·39	1·33	1·35	Major histocompatibility complex, class II, DM alpha
203932_at	*HLA-DMB*	0·64	0·31	2·02	1·36	Major histocompatibility complex, class II, DM beta
211991_s_at	*HLA-DPA1*	0·50	0·14	1·54	1·50	Major histocompatibility complex, class II, DP alpha 1
212671_s_at	*HLA-DQA1*	0·44	0·23	1·56	2·56	Major histocompatibility complex, class II, DQ alpha 1
211656_x_at	*HLA-DQB1*	0·63	0·48	1·37	7·07	Major histocompatibility complex, class II, DQ beta 1
210982_s_at	*HLA-DRA*	0·58	0·37	1·50	1·42	Major histocompatibility complex, class II, DR alpha
208306_x_at	*HLA-DRB1*	0·51	0·24	1·49	1·61	Major histocompatibility complex, class II, DR beta 3
204670_x_at	*HLA-DRB5*	0·63	0·22	1·47	1·37	Major histocompatibility complex, class II, DR beta 5
211634_x_at	*IGHV1-69*	0·69	0·77	1·23	1·99	Immunoglobulin heavy variable 1–69
211645_x_at	*IgK*	0·15	0·49	1·51	6·62	Immunoglobulin kappa light chain (IGKV)
221651_x_at	*IGKC*	0·46	0·68	1·32	5·57	Immunoglobulin kappa constant
215379_x_at	*IGLC2*	0·62	0·41	1·38	4·26	Immunoglobulin lambda joining 2
209031_at	*IGSF4*	0·50	0·03	2·33	1·50	Immunoglobulin superfamily, member 4
205686_s_at	*CD86*	0·70	0·23	1·30	1·39	CD86 antigen (CD28 antigen ligand 2, B7-2 antigen)
204698_at	*ISG20*	0·68	0·49	1·32	1·64	Interferon stimulated exonuclease gene, 20 kDa
213915_at	*NKG7*	0·72	0·42	1·28	2·31	Natural killer cell group 7 sequence
Cell growth and maintenance						
201334_s_at	*ARHGEF12*	0·74	0·50	1·26	1·96	Rho guanine nucleotide exchange factor (GEF) 12
230292_at	*CHC1L*	0·70	0·56	1·30	2·02	Regulator of chromosome condensation (RCC1)
205081_at	*CRIP1*	0·56	0·73	1·27	1·75	Cysteine-rich protein 1 (intestinal)
31874_at	*GAS2L1*	0·77	0·52	1·23	2·35	Growth arrest-specific 2 like 1
202364_at	*MXI1*	0·43	0·73	1·27	1·44	MAX interactor 1
219304_s_at	*PDGFD*	0·65	0·71	1·29	3·68	Platelet-derived growth factor D
213397_x_at	*RNASE4*	0·64	0·46	1·36	2·21	Ribonuclease, RNase A family, 4
213566_at	*RNASE6*	0·69	0·39	1·49	1·31	Ribonuclease, RNase A family, k6
219077_s_at	*WWOX*	0·40	0·78	1·25	1·22	WW domain containing oxidoreductase
Cytokine and chemokine						
207861_at	*CCL22*	0·76	0·52	1·24	2·47	Chemokine (C–C motif) ligand 22
238750_at	*CCL28*	0·74	0·45	1·26	1·41	Chemokine (C–C motif) ligand 28
1555759_a_at	*CCL5*	0·71	0·23	1·29	1·92	Chemokine (C–C motif) ligand 5
208304_at	*CCR3*	0·50	0·12	1·50	2·35	Chemokine (C–C motif) receptor 3
205898_at	*CX3CR1*	0·30	0·20	1·70	4·16	Chemokine (C–X3–C motif) receptor 1
204533_at	*CXCL10*	0·80	0·16	1·20	2·53	Chemokine (C–X–C motif) ligand 10
219255_x_at	*IL-17RB*	0·73	0·04	1·27	1·29	Interleukin 17 receptor B
206148_at	*IL-3RA*	0·60	0·54	2·46	1·40	Interleukin 3 receptor, alpha (low affnity)
226333_at	*IL-6R*	0·22	0·79	1·21	2·43	Interleukin-6 receptor
206693_at	*IL-7*	0·09	0·54	1·46	5·86	Interleukin-7
Signal transduction						
204497_at	*ADCY9*	0·76	0·40	1·24	2·40	Adenylate cyclase 9
206170_at	*ADRB2*	0·58	0·35	1·42	3·97	Adrenergic, beta-2-, receptor, surface
202096_s_at	*BZRP*	0·50	0·54	1·59	1·46	Benzodiazapine receptor (peripheral)
230464_at	*EDG8*	0·04	0·09	1·91	2·42	Endothelial differentiation, sphingolipid G-protein-coupled receptor 8
223423_at	*GPR160*	0·54	0·68	1·40	1·32	G protein-coupled receptor 160
227769_at	*GPR27*	0·07	0·08	1·92	244	G protein in-coupled receptor 27
210095_s_at	*IGFBP3*	0·27	0·20	1·73	5·25	Insulin-like growth factor binding protein 3
38671_at	*PLXND1*	0·08	0·65	1·35	2·57	Plexin D1
226101_at	*PRKCE*	0·56	0·43	1·72	1·44	Protein kinase C. epsilon
232629_at	*PROK2*	0·01	0·13	1·87	2·09	Prokineticin 2

Table 4. Continued

Affi ID	Gene abbreviation	Fold change CB 1	CB 2	PB 1	PB 2	Gene name
203329_at	*PTPRM*	0·36	0·62	1·38	1·93	Protein tyrosine phosphatase, receptor type, M
204731_at	*TGFBR3*	0·78	0·55	1·22	2·04	Transforming growth factor, beta receptor III (betaglycan, 300 kDa)
Transcription						
203129_s_at	*KIF5C*	0·67	0·09	1·33	3·43	Kinesin family member 5C
213906_at	*MYBL1*	0·75	0·51	1·25	3·63	V-myb myeloblastosis viral oncogene homologue (avian)-like 1
209815_at	*PTCH*	0·59	0·27	1·41	4·17	Patched homologue (*Drosophila*)
213891_s_at	*TCF4*	0·74	0·65	2·06	1·26	Transcription factor 4
238520_at	*TRERFI*	0·70	0·77	1·23	2·30	Transcriptional regulating factor 1
203603_s_at	*ZFHX1B*	0·74	0·61	1·26	3·63	Zinc finger homobox 1b
213218_at	*ZNF187*	0·74	0·69	1·26	1·76	Zinc finger protein 187
221123_x_at	*ZNF395*	0·38	0·71	1·63	1·29	Zinc finger protein 395

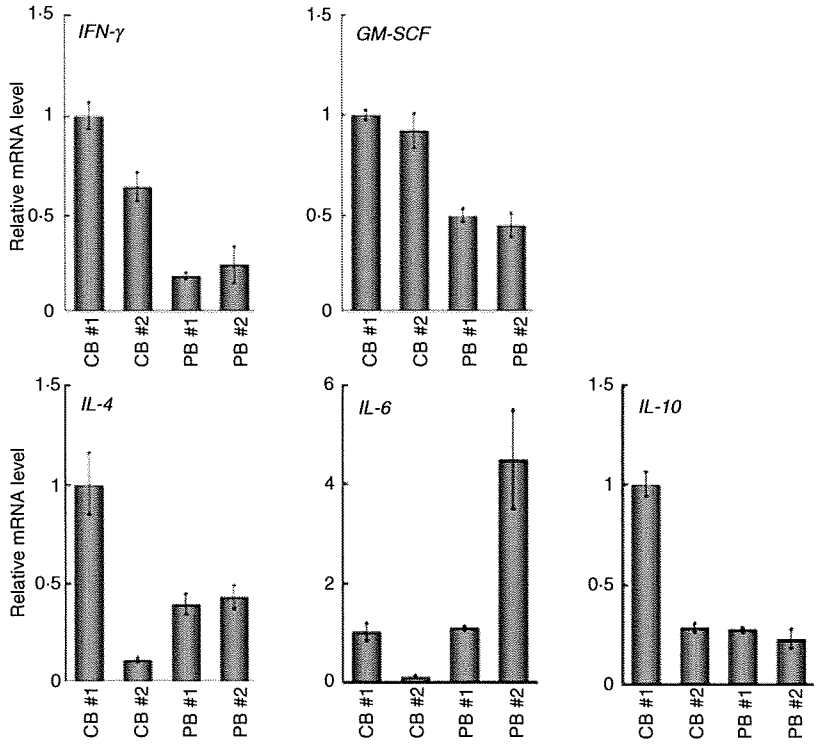

Figure 2. Quantitative polymerase chain reaction (PCR) analysis of the genes related to the T helper type 1 (Th1) and Th2 phenotypes. The expression of the genes indicated was examined by real-time reverse transcriptase (RT)-PCR using the same sample specimens as in Fig 1. Data are normalized to the mRNA level in PB 1 which is arbitrarily set to 1. The signal intensity was normalized using that of a control housekeeping gene [the human glyceraldehyde-3-phosphate dehydrogenase (*GAPDH*) gene]. Data are relative values with the standard deviation (SD) for triplicate wells.

significantly higher in PB-derived $CD4^+$ T cells in comparison with equivalent CB-derived $CD4^+$ T cells at 1 week ($P < 0{\cdot}05$) but not at 2 weeks (Fig. 6).

Discussion

Although it is generally believed that there are functional differences between CB and PB lymphocytes, the details are obscure. For instance, Azuma *et al.*[13] reported that the phenotype and function of expanded CB lymphocytes were essentially equivalent to those of expanded PB lymphocytes when evaluated in *in vitro* experiments. In the present study, however, we have shown that CB-derived $CD4^+$ T cells revealed a distinct expression profile of genes important for the function of particular T-cell subsets compared with PB-derived $CD4^+$ T cells.

$CD4^+$ T cells can be classified into distinct subsets, including effector $CD4^+$ cells and Tregs, according to their functional characteristics as well as differentiation profiles.[14–16] Typically, effector $CD4^+$ T cells have been further divided into two distinct lineages on the basis of their cytokine production profiles, namely Th1 and Th2. Th1 cells producing cytokines such as IL-2, IFN-γ and GM-CSF have evolved to enhance the eradication of intracellular pathogens and are thought to be potent activators of cell-mediated immunity. In contrast, Th2

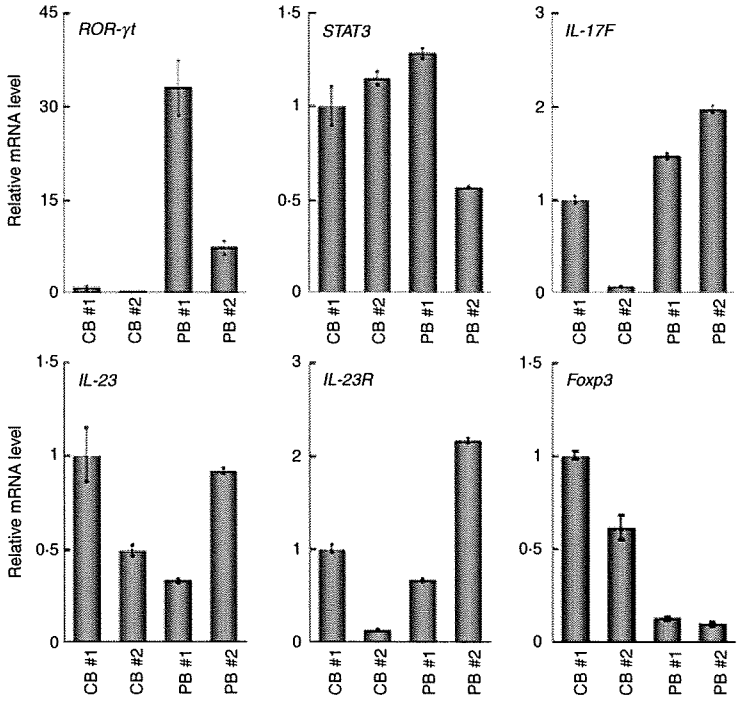

Figure 3. Quantitative polymerase chain reaction (PCR) analysis of the forkhead box protein 3 gene (*FOXP3*) and the genes related to the secretion of interleukin (IL)-17. The expression of the genes indicated was examined as in Fig 2. Data are normalized to the mRNA level in peripheral blood sample 1 (PB 1) as in Fig.2. The signal intensity was normalized using that of a control housekeeping gene [the human glyceraldehyde-3-phosphate dehydrogenase (*GAPDH*) gene]. Data are relative values with the standard deviation for triplicate wells.

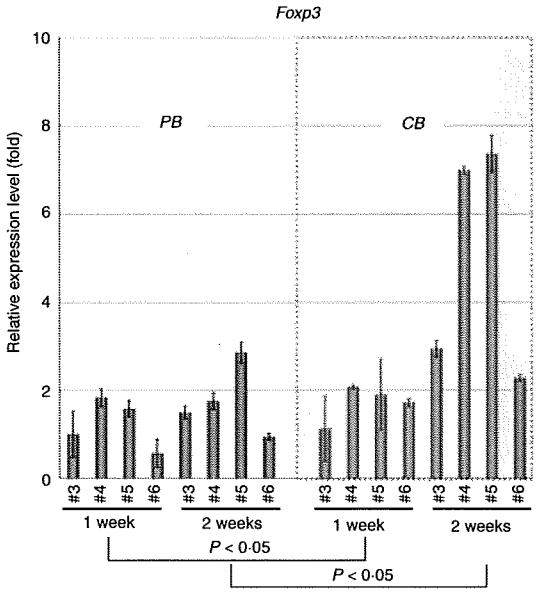

Figure 4. Quantitative polymerase chain reaction (PCR) analysis of the forkhead box protein 3 gene (*FOXP3*) in additional samples. Additional peripheral blood (PB) and cord blood (CB) samples were prepared and RNAs were extracted at 1 and 2 weeks. The expression of the *FOXP3* gene was examined as in Fig. 2. Data are normalized to the mRNA level in the sample of PB 3 at 1 week, which is arbitrarily set to 1. The signal intensity was normalized using that of a control housekeeping gene (the human β-actin gene). Data are relative values with the standard deviation for triplicate wells. The data were analysed statistically and *FOXP3* gene expression in CB-derived $CD4^+$ T cells was found to be significantly higher in comparison with equivalent PB-derived $CD4^+$ T cells at both 1 week ($P < 0{\cdot}05$) and 2 weeks ($P < 0{\cdot}05$).

cells secreting cytokines such as IL-4, IL-5, IL-6, IL-9 and IL-13 have evolved to enhance the elimination of parasitic infections and are thought to be potent activators of B-cell immunoglobulin E production, eosinophil recruitment, and mucosal expulsion. Th1-type responses to self or commensal floral antigens can promote tissue destruction and chronic inflammation, whereas dysregulated Th2-type responses can cause allergy and asthma. The development of Th1 is specified by the transcription factor T-bet (also known as Tbx-21) and master regulators of Th2 differentiation are GATA-3 and c-maf.

As shown in Fig. 2 and Table 2, the gene expression profiles of CB- and PB-derived $CD4^+$ T cells revealed no significant differences regarding cytokines related to the definition of Th1 and Th2, with the exceptions of IFN-γ and GM-CSF. The mRNA levels of IFN-γ and GM-CSF tended to be higher in CB-derived $CD4^+$ T cells than in PB-derived $CD4^+$ T cells. The mRNA expression of the transcription factors T-bet, GATA-3 and c-maf, which regulate Th1 and Th2 cell differentiation, did not differ significantly between CB- and PB-derived $CD4^+$ T cells.

In addition to Th1 and Th2 cells, IL-17 (also known as IL-17A)-producing T lymphocytes have been recently shown to comprise a distinct third subset of T helper cells, termed Th17 cells, in the mouse immune system. Th17 cells exhibit pro-inflammatory characteristics and act as major contributors to autoimmune disease. A number of experiments using animal models support a significant role for IL-17 in the response to allografts.[14,16,17] There is as yet no direct evidence for the existence of discrete Th17 cells in humans, although

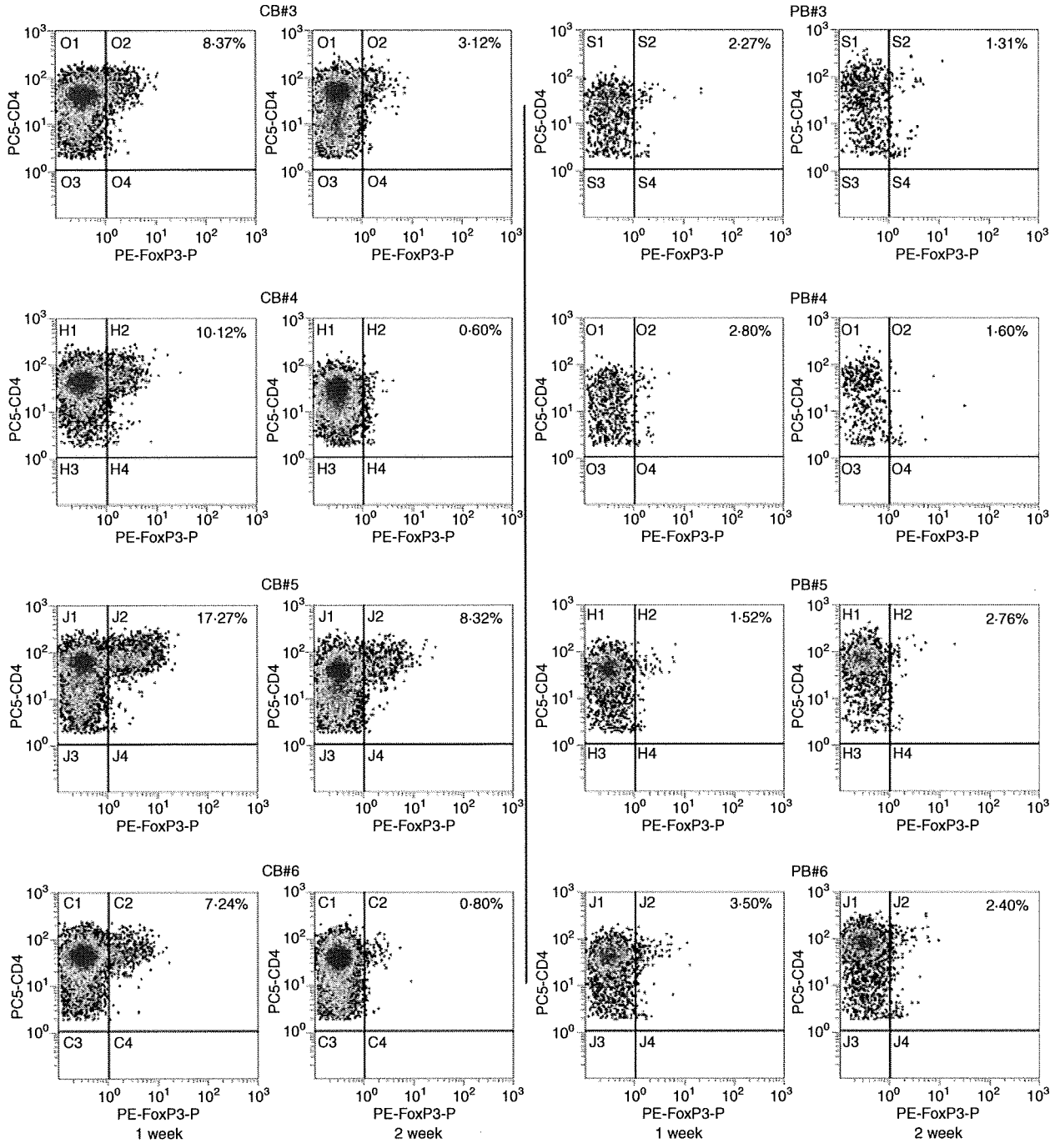

Figure 5. Protein expression of forkhead box protein 3 (Foxp3) in activated $CD4^+$ T cells. The protein expression of Foxp3 in same sample specimens as in Fig. 4 was examined by flow cytometry. The CD4 versus Foxp3 cytogram of the population gated with $CD3^+$ and $CD4^+$ in each sample is presented.

helper T cells secreting IL-17 have clearly been detected in the human immune system.[18] Several studies have shown a correlation between allograft rejection and IL-17. For example, IL-17 levels are elevated in human renal allografts during subclinical rejection and there are detectable mRNA levels in the urinary mononuclear cell sediments of these patients.[19,20] In human lung organ transplantation, IL-17 levels have also been reported to be elevated during acute rejection.[21] Interestingly, in this study, most of the PB-derived $CD4^+$ T-cell samples expressed higher levels of IL-17 mRNA than the CB-derived $CD4^+$ T-cell samples, suggesting that PB-derived $CD4^+$ T cells frequently include potent IL-17-secreting T cells.

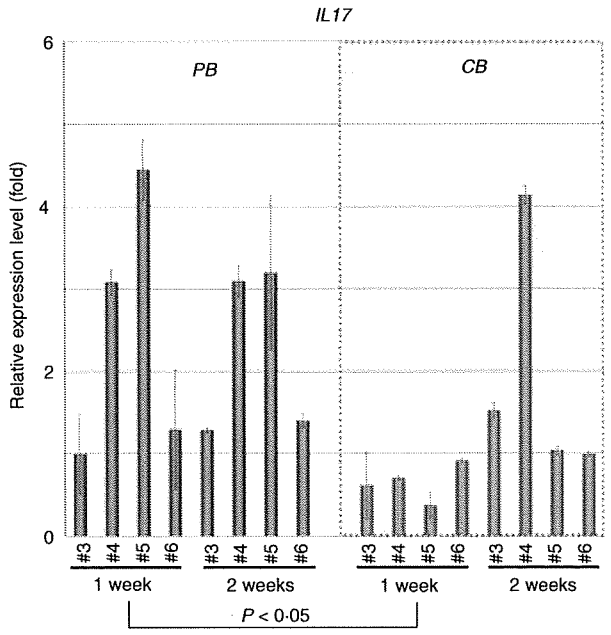

Figure 6. Quantitative polymerase chain reaction (PCR) analysis of interleukin (IL)-17 in additional samples. The expression of the *IL-17* gene in the same sample specimens as in Fig. 4 was examined and presented as in Fig 2. The data were analysed statistically and *IL-17* gene expression in peripheral blood (PB)-derived $CD4^+$ T cells was found to be significantly higher in comparison with equivalent CB-derived $CD4^+$ T cells at 1 week ($P < 0{\cdot}05$) but not at 2 weeks.

Th17 cells expand independently of T-bet or STAT-1. Ivanov *et al.*[22] have shown that the orphan nuclear receptor RORγt is the key transcription factor orchestrating the differentiation of the effector lineage. RORγt induces transcription of the gene encoding IL-17 in naïve $CD4^+$ T helper cells and is required for its expression in response to IL-6 and transforming growth factor (TGF)-β, the cytokines known to induce IL-17 expression. IL-23 is also involved in Th17 cell differentiation, but naïve T cells do not have the IL-23 receptor and are relatively refractory to IL-23 stimulation.[23,24] Although IL-23 seems to be an essential survival factor for Th17 cells, it is not required during their differentiation. It has been suggested that IL-23R expression is up-regulated on RORγt$^+$ Th17 cells in an IL-6-dependent manner. IL-23 may therefore function subsequent to IL-6/TGF-β-induced commitment to the Th17 lineage to promote cell survival and expansion and, potentially, the continued expression of IL-17 and other cytokines that characterize the Th17 phenotype. As presented in Fig. 3, the expression of the *RORγt* gene was significantly weaker in CB-derived $CD4^+$ T cells, whereas the expression of genes encoding IL-23 and the IL-23 receptor did not differ significantly between the $CD4^+$ T cells. Based on the above findings of others, it is possible that the low-level expression of the *RORγt* gene in CB-derived $CD4^+$ T cells is responsible for the absence of *IL-17* mRNA expression in those cells.

Tregs are another functional subset of T cells having anti-inflammatory properties and can cause quiescence of autoimmune diseases and prolongation of transplant function. *In vitro*, Tregs have the ability to inhibit the proliferation and production of cytokines by responder ($CD4^+$ $CD25^-$ and $CD8^+$) T cells subjected to polyclonal stimuli, as well as to down-regulate the responses of $CD8^+$ T cells, NK cells and $CD4^+$ cells to specific antigens.[25,26] These predicates translate *in vivo* to a great number of functions other than the maintenance of tolerance to self-components (prevention of autoimmune disease), such as the ability to prevent transplant rejection. Indeed, donor-specific Tregs can prevent allograft rejection in some models of murine transplant tolerance through a predominant effect on indirect alloresponses.

Foxp3 is thought to be responsible for the development of the Treg population and can act as a phenotypic marker of this fraction.[27] Tregs constitutively express CTLA-4 and there are suggestions that signalling through this pathway may be important for their function, as antibodies to CTLA-4 can inhibit Treg-mediated suppression.[28] As shown above, most of the CB-derived $CD4^+$ T cells were found to express either the *FOXP3* gene or the Foxp3 protein at higher levels compared with PB-derived $CD4^+$ T cells, suggesting that CB-derived $CD4^+$ T cells frequently include a potent Treg population.

As described above, *IL-17* mRNA was more detectable in PB-derived $CD4^+$ cells while *FOXP3* mRNA expression was higher in CB-derived $CD4^+$ cells. Post-transcriptional regulation, as well as differences in mRNA and protein turnover rates, can cause discrepancies between mRNA and protein expression and thus the differences observed in the mRNA expression do not necessary directly indicate those in protein expression.[29] Indeed, we observed some discrepancy between the levels of mRNA and protein with regard to Foxp3 expression in CB-derived $CD4^+$ T cells, as presented above. Nevertheless, changes in mRNA expression are mediated by the alteration of transcriptional regulation, and thus should indicate the differentiation ability of the cells. Therefore, our data indicate that CB-derived $CD4^+$ T cells tend frequently to include potent Tregs, while PB-derived $CD4^+$ T cells tend to include potent IL-17-secreting cells. As described above, DLI with donor CB-derived activated $CD4^+$ T cells is currently becoming established as a routine therapeutic strategy in Japan. It has been proposed that the skewing of responses towards Th17 or Th1 cells and away from Tregs may be responsible for the development and/or progression of autoimmune diseases or acute transplant rejection, and it may thus also be speculated that CB-derived $CD4^+$ T cells are more appropriate for DLI than PB-derived $CD4^+$ T cells.

However, our data also indicate the presence of individual, donor-dependent variations in the characteristics of activated $CD4^+$ T cells derived from CB and PB. More-

over, activated $CD4^+$ T cells do not consist of a single population and should include several distinct functional subsets of $CD4^+$ T cells. Therefore, it is important to clarify the characteristics of activated $CD4^+$ T cells in each preparation to predict the therapeutic effect of DLI in each clinical case.

In summary, our findings demonstrate a difference in gene expression between activated $CD4^+$ T cells derived from CB and those derived from PB. The higher level of *FOXP3* gene expression and the lower level of *IL-17* gene expression in CB-derived $CD4^+$ T cells may indicate that these cells have potential as immunomodulators in DLI therapy. Further detailed analysis should reveal the advantages of activated $CD4^+$ T cells from CB in DLI.

Acknowledgements

We thank the Tokyo Cord Blood Bank for the distribution of cord blood for research use. This work was supported by a grant from the Japan Health Sciences Foundation for Research on Publicly Essential Drugs and Medical Devices (KHC2032), Health and Labour Sciences Research Grants (the 3rd term comprehensive 10-year strategy for cancer control H19-010, Research on Children and Families H18-005, Research on Human Genome Tailor-made and Research on Publicly Essential Drugs and Medical Devices H18-005), and a Grant for Child Health and Development from the Ministry of Health, Labour and Welfare of Japan. It was also supported by CREST, JST.

Disclosures

No competing personal or financial interests exist for any of the authors in relation to this manuscript.

References

1 Loren AW, Porter DL. Donor leukocyte infusions after unrelated donor hematopoietic stem cell transplantation. *Curr Opin Oncol* 2006; **18**:107–14.

2 Roush KS, Hillyer CD. Donor lymphocyte infusion therapy. *Transfus Med Rev* 2002; **16**:161–76.

3 Alyea EP, Soiffer RJ, Canning C *et al.* Toxicity and efficacy of defined doses of CD4(+) donor lymphocytes for treatment of relapse after allogeneic bone marrow transplant. *Blood* 1998; **91**:3671–80.

4 Giralt S, Hester J, Huh Y *et al.* CD8-depleted donor lymphocyte infusion as treatment for relapsed chronic myelogenous leukemia after allogeneic bone marrow transplantation. *Blood* 1995; **86**:4337–43.

5 Tomizawa D, Aoki Y, Nagasawa M *et al.* Novel adopted immunotherapy for mixed chimerism after unrelated cord blood transplantation in Omenn syndrome. *Eur J Haematol* 2005; **75**:441–4.

6 Cohena Y, Nagler A. Hematopoietic stem-cell transplantation using umbilical-cord blood. *Leuk Lymphoma* 2003; **44**:1287–99.

7 Parmar S, Robinson SN, Komanduri K *et al.* Ex vivo expanded umbilical cord blood T cells maintain naive phenotype and TCR diversity. *Cytotherapy* 2006; **8**:149–57.

8 Robinson KL, Ayello J, Hughes R, van de Ven C, Issitt L, Kurtzberg J, Cairo MS. Ex vivo expansion, maturation, and activation of umbilical cord blood-derived T lymphocytes with IL-2, IL-12, anti-CD3, and IL-7. Potential for adoptive cellular immunotherapy post-umbilical cord blood transplantation. *Exp Hematol* 2002; **30**:245–51.

9 Miyagawa Y, Okita H, Nakaijima H *et al.* Inducible expression of chimeric EWS/ETS proteins confers Ewing's family tumor-like phenotypes to human mesenchymal progenitor cells. *Mol Cell Biol* 2008; **28**:2125–37.

10 Werlen G, Hausmann B, Naeher D, Palmer E. Signaling life and death in the thymus: timing is everything. *Science* 2003; **299**:1859–63.

11 Riley JL, June CH. The CD28 family: a T-cell rheostat for therapeutic control of T-cell activation. *Blood* 2005; **105**:13–21.

12 Woo EY, Yeh H, Chu CS, Schlienger K, Carroll RG, Riley JL, Kaiser LR, June CH. Cutting edge: regulatory T cells from lung cancer patients directly inhibit autologous T cell proliferation. *J Immunol* 2002; **168**:4272–6.

13 Azuma H, Yamada Y, Shibuya-Fujiwara N *et al.* Functional evaluation of ex vivo expanded cord blood lymphocytes: possible use for adoptive cellular immunotherapy. *Exp Hematol* 2002; **30**:346–51.

14 Afzali B, Lombardi G, Lechler RI, Lord GM. The role of T helper 17 (Th17) and regulatory T cells (Treg) in human organ transplantation and autoimmune disease. *Clin Exp Immunol* 2007; **148**:32–46.

15 Castellino F, Germain RN. Cooperation between CD4+ and CD8+ T cells: when, where, and how. *Annu Rev Immunol* 2006; **24**:519–40.

16 Reiner SL. Development in motion: helper T cells at work. *Cell* 2007; **129**:33–6.

17 Bi Y, Liu G, Yang R. Th17 cell induction and immune regulatory effects. *J Cell Physiol* 2007; **211**:273–8.

18 Fossiez F, Djossou O, Chomarat P *et al.* T cell interleukin-17 induces stromal cells to produce proinflammatory and hematopoietic cytokines. *J Exp Med* 1996; **183**:2593–603.

19 Loong CC, Hsieh HG, Lui WY, Chen A, Lin CY. Evidence for the early involvement of interleukin 17 in human and experimental renal allograft rejection. *J Pathol* 2002; **197**:322–32.

20 Van Kooten C, Boonstra JG, Paape ME *et al.* Interleukin-17 activates human renal epithelial cells in vitro and is expressed during renal allograft rejection. *J Am Soc Nephrol* 1998; **9**:1526–34.

21 Vanaudenaerde BM, Dupont LJ, Wuyts WA *et al.* The role of interleukin-17 during acute rejection after lung transplantation. *Eur Respir J* 2006; **27**:779–87.

22 Ivanov II, McKenzie BS, Zhou L, Tadokoro CE, Lepelley A, Lafaille JJ, Cua DJ, Littman DR. The orphan nuclear receptor RORgammat directs the differentiation program of proinflammatory IL-17+ T helper cells. *Cell* 2006; **126**:1121–33.

23 Langrish CL, Chen Y, Blumenschein WM *et al.* IL-23 drives a pathogenic T cell population that induces autoimmune inflammation. *J Exp Med* 2005; **201**:233–40.

24 Oppmann B, Lesley R, Blom B *et al.* Novel p19 protein engages IL-12p40 to form a cytokine, IL-23, with biological activities similar as well as distinct from IL-12. *Immunity* 2000; **13**: 715–25.

25 Dieckmann D, Plottner H, Berchtold S, Berger T, Schuler G. Ex vivo isolation and characterization of CD4(+) CD25(+) T cells with regulatory properties from human blood. *J Exp Med* 2001; **193**:1303–10.

26 Wing K, Lindgren S, Kollberg G, Lundgren A, Harris RA, Rudin A, Lundin S, Suri-Payer E. CD4 T cell activation by myelin oligodendrocyte glycoprotein is suppressed by adult but not cord blood CD25+ T cells. *Eur J Immunol* 2003; **33**:579–87.

27 Wan YY, Flavell RA. Identifying Foxp3-expressing suppressor T cells with a bicistronic reporter. *Pro Natl Acad Sci USA* 2005; **102**:5126–31.

28 Read S, Greenwald R, Izcue A, Robinson N, Mandelbrot D, Francisco L, Sharpe AH, Powrie F. Blockade of CTLA-4 on CD4+ CD25+ regulatory T cells abrogates their function in vivo. *J Immunol* 2006; **177**:4376–83.

29 Hack CJ. Integrated transcriptome and proteome data: the challenges ahead. *Brief Funct Genomic Proteomic* 2004; **3**:212–9.

Pathology International

Pathology International 2009; **59**: 332–344 doi:10.1111/j.1440-1827.2009.02375.x

Case Report

Follicular dendritic cell sarcoma with microtubuloreticular structure and virus-like particle production *in vitro*

Yuri Ono,[1] Kazuo Terashima,[6,8] Aimin Liu,[3] Munehiro Yokoyama,[5] Kazuhiro Yokoshima,[2] Miki Mizukami,[7] Ken Watanabe,[7] Yoko Mochimaru,[6,7] Tohru Furusaka,[9] Norio Shimizu,[7] Naoki Yamamoto,[8] Toshiyuki Ishiwata,[1] Yuuichi Sugisaki,[4] Toshiaki Yagi[2] and Zenya Naito[1]

Department of [1]Pathology, Integrative Oncological Pathology, and [2]Oto-rhino-laryngology, Head and Neck Surgery, [3]Central Institute of Electroscopic Research and [4]Division of Surgical Pathology, Nippon Medical School, [5]Division of Surgical Pathology, Tokyo Metropolitan Police Hospital, [6]Departments of Comprehensive Pathology and [7]Virology, Division of Medical Science, Medical Research Institute, Tokyo Medical and Dental University, [8]National Institute Infectious Diseases, AIDS Research Center and [9]Department of Oto-rhino-laryngology, Nihon University Hospital, Tokyo, Japan

Neoplasm of follicular dendritic cells (FDC), follicular dendritic cell sarcoma (FDCS), is a rare tumor of intermediate to high-grade malignancy in lymph nodes and visceral organs. Reported herein is a case of FDCS arising from cervical lymph nodes in a 16-year-old Japanese boy, who died of the disease 3 years after diagnosis. The tumor cells were pale eosinophilic and elongated with euchromatic nuclei and were positive for CD21, clusterin, and CNA-42 on immunohistochemistry, as well as desmosome-like junctions on electron microscopy. The presence of microtubuloreticular structures (MTRS) in the tumor cells and associated lymphocytes characterized this case, suggesting some viral infection, although qualitative polymerase chain reaction of genomic and complementary DNA obtained from the tumor failed to demonstrate any viral infection at the laboratory level. The stimulation of dispersed tumor cells and peripheral blood mononuclear cells with mAb to CD3 and interleukin-2 was attempted; and the cell line established by the authors (FDCS-Sa) was stimulated with iododeoxyuridine. Virus-like particles (VLP) were successfully induced from each cellular source. The VLP, 100 nm in diameter, showed an electron-dense thorny envelope and granular core. This is the first case of FDCS with MTRS accompanying VLP production *in vitro*.

Key words: follicular dendritic cell sarcoma, follicular dendritic cells, microtubuloreticular structure, virus-like particles

Correspondence: Yuri Ono, MD, Department of' Pathology, Integrative Oncological Pathology, Nippon Medical School, Sendagi 1-1-5, Bunkyo-ku, Tokyo 113-8603, Japan. Email: yuri@nms.ac.jp

Received 29 September 2008. Accepted for publication 12 January 2009.

Different from ordinary dendritic cells (DC) present in the entire body, follicular dendritic cells (FDC) are confined to the lymph follicles and germinal centers (GC) of lymphoid tissue, forming a network to trap antigen/immune complexes and playing an indispensable role in the secondary immune response. Their ontogeny, however, remains controversial, in contrast to monocyte-derived DC.[1–3] First, we will briefly review studies on FDC in various diseases. Long-term trapping of virus and/or viral products by FDC is observed in various autoimmune diseases of mice and humans, including systemic lupus erythematosus,[4,5] and in HIV-1 infection. FDC trap HIV-1 virus in the long term, which infect T cells in GC not only in the form of immune complexes but also in native forms in the prodromal stage with no specific antibody.[5,6] Keele *et al.* showed that FDC entirely contribute to the transformation of HIV-1 to its variant forms.[7] The integration of HIV-1 into FDC, however, remains disputable.[6,8,9] In prion disease FDC were thought to be the initial site for abnormal prion protein (such as seen in scrapie disease and other prion disease; PrP^{Scr}) anchorage and replication,[10] before its transmission to the central nervous system via the autonomic nervous system.[11]

FDC reactively proliferate in association with various neoplastic diseases such as mantle cell lymphoma,[12] Castleman disease,[13] and angioimmunoblastic T-cell lymphoma (AITL).[14–17] They proliferate extrafollicularly among lymphoma cells.[18,19] In the latter, cytokines such as CD40, transforming growth factor-α, and interleukin (IL)-1β were suggested to be responsible for inducing hyperplasia of FDC or development of FDC from its precursor.[20,21]

Neoplasm of FDC, follicular dendritic cell sarcoma (FDCS), is a rare neoplasm of high-grade malignancy arising in various organs including lymph nodes, soft tissue, retroperitoneum and liver. There have been 100–150 cases reported

worldwide, 17 of which were from Japan, including the present case. The patient age varies from 9 to 82 years (using PubMed and MEDLINE (ICHU) search).[22–25]

We report a case of FDCS arising from the cervical lymph node of a 16-year-old Japanese boy, which recurred 19 months later, with a clinical course of 34 months from disease diagnosis to death due to respiratory failure, with metastasis to supramediastinum and lungs. This case is characterized by the presence of microtubuloreticular structures (MTRS) in both tumor cells and associated lymphocytes, mostly T cells, as well as by *in vitro* production of virus-like particles (VLP) by the tumor cells and lymphocytes.

We established a cell line of FDCS designated as FDCS-Sa, which is the second cell line as far as we know (Katano H., pers. comm., 1999). VLP were also replicated by FDCS-Sa when stimulated by iododeoxyuridine (IdUrd). In the discussion, we focus on the relationship between MTRS and VLP.

CLINICAL SUMMARY

A 16-year-old Japanese boy was referred to Nippon Medical School Hospital with a 3 month-history of lymph nodal swelling on the left side of his neck. Magnetic resonance imaging indicated an irregularly lobulated solid tumor located in the left parapharyngeal space and enhanced by injected gadolinium. Fine-needle aspiration (FNA) demonstrated dual cell populations of malignant medium to large cells of unknown origin and small lymphocytes (Fig. 1a). Excisional biopsy was performed. The resected tumor was observed to be an elastic soft, well-circumscribed mass, 35 mm × 50 mm in diameter and diagnosed as FDCS on the basis of histopathological, immunohistochemical, and ultrastructual findings. Clinical laboratory data on the first admission showed no particular finding of note except for a slight elevation of LDH. This patient had neither medical history of autoimmune diseases nor symptomatic EBV infection. His serological antibodies to EBV (EBV capsid antigen (EBVCA)-IgG, EBVCA-IgM, EBVCA-IgA, early antigen-diffuse and restrict complex (EBEA-DR-1), EBV nuclear antigen (EBNA)) were within normal limits.

Eleven months later at postoperative follow up, even though his performance status was fine, hematological analysis indicated atypical large mononuclear cells, comprising <1.0% of peripheral blood mononuclear cells (PBMNC), forming clusters of atypical large cells or tumor cells when cultured. This episode, however, was not followed by further detailed analysis. Nineteen months after the first operation he had recurrent localized tumors up to 3 cm in diameter and underwent neck dissection at second operation. On histopathology the tumor cells had more distinct sarcomatous features, indicating higher grade malignancy. Afterwards, chest X ray indicated metastasis to the supramediastinum and lungs, which caused fatal dyspnea. The patient died 2 years 10 months after diagnosis. Autopsy was not performed.

MATERIALS AND METHODS

The protocols and all examinations followed the ethics guidelines of Nippon Medical School, and Tokyo Medical and Dental University, with informed consent of the patient's family.

Cytology

Free-hand FNA was performed on the tumor using 22 G needles at the Division of Surgical Pathology, Nippon Medical School, Tokyo, Japan. Aspirated materials were smeared on glass slides and fixed in 95% ethanol. The residual material in the syringe was rinsed out and fixed in 10% neutral buffered formalin for subsequent cell block preparation. Slides from aspirates were stained with the Papanicolaou stain, and unstained smears were used for immunohistochemistry.

Three-color flow cytometry

For three-color flow cytometry (FCM), cell suspensions were obtained by straining fresh specimens obtained from the second operation. Cells were processed in accordance with the manufacturer's protocol (Cytometry Section, BML, Tokyo, Japan).

All the antibodies used for three-color FCM were purchased from Becton-Dickinson, San Jose, CA, USA, Japan. Fluorescein isothiocyanate, phycoerythrin, and 7-aminoactinomycin D were used as cell cycle dyes. The cells were analyzed on a FACSCaliber flow cytometer (Becton-Dickinson). Scattergram and fluorescence signals were collected in the linear mode and logarithmic scale, respectively.[26]

Histopathology, immunohistochemistry and electron microscopy

One half of the extirpated tumor was fixed in 10% neutral buffered formalin and embedded in paraffin at the Division of Surgical Pathology, Nippon Medical School, Tokyo, Japan. The another half was frozen for immunostaining and molecular biological analysis. Formalin-fixed paraffin-embedded (FFPE) sections, 4 μm thick, were mounted on silane-coated slides. Immunohistochemistry was performed using the antigen retrieval method with 0.05% citraconic anhydride

solution, pH7.4 (Immunosaver; Nissin EM, Tokyo, Japan) and the Ventana DAB Universal Kit and an automated stainer (NexES IHC, Ventana Medical Systems; Yokohama, Japan).[27] CD 21 and clusterin were immunostained according to the manufacturer's methods. Table 1 lists all the antibodies, along with the antibody clone and dilution, the antigenic retrieval method used, and incubation time.

CD23, DRC-1, CAN-42, S-100-α, CD137, and tyrosine hydroxidase were immunostained with monoclonal and polyclonal antibodies as described in the following section, using the direct or labeled streptoavidine (LSAB) method with dewaxed sections after dipping in antigen-retrieval LAB solution (Polyscience, Niles, IL, USA) and using cells cultured in chamber slides or frozen sections after acetone fixation at the Department of Comprehensive Pathology, and Department of Virology, Division of Medical Science, Medical Research Institute, Tokyo Medical and Dental University, Tokyo, Japan (Table 1). GM1 ganglioside (GM1) was stained with HRP-labeled CTB (Molecular Probes and Invitrogen, Carlsbad, CA, USA).

EBV-encoded early nuclear RNA (EBER) *in situ* hybridization (ISH) was performed using an Alpha DIG-AP EBV-EBER kit (HKD38101, Nichirei, Tokyo, Japan). Positive controls were included in all runs and all slides were analyzed by two pathologists (Y.O. and M.Y.).

Electron microscopy

Specimens were obtained from the first and second operations at the Division of Surgical Pathology, Nippon Medical School, Tokyo, Japan. A small portion of fresh tissue was fixed in 2.5% glutaraldehyde and post-fixed in 1% osmium tetroxide, dehydrated in a graded series of alcohol, and embedded in Epon 812. Ultrathin sections were stained with uranyl acetate and lead citrate, and observed under Hitachi 7200 and 7500 electron microscopes (Hitachi, Tokyo, Japan) equipped with an AMT CCD camera system (Advanced Microscopy Techniques, Danvers, MA, USA).

Specimens were obtained from peripheral blood sampled between two operations. After centrifugation of heparinized blood samples, the plasma was replaced with a 2.5% glutaraldehyde for fixation. After hardening, the buffy coat disk was removed and minced into small pieces in accordance with a method described by Anderson.[28] Cells cultured on tissue disk (13 mm in diameter, Sumitomo Plastic, Tokyo, Japan) in 24-well culture dishes were fixed *in situ* with 2.5% glutaraldehyde/0.1 mol/L phosphate buffer and processed for Epon embedding.

Cell culture

Specimens obtained from the second operation were processed for cell culture at the Department of Comprehensive Pathology, and Department of Virology, Division of Medical Science, Medical Research Institute, Tokyo Medical and Dental University, Tokyo, Japan, following collagenase treatment (Wako Pure Chemicals, Tokyo, Japan), in DMEM plus 20% FCS with epithelial cell growth factor (ECGF) and heparin sulfate. Cells were then serially replated to obtain an FDCS strain, designated as FDCS-Sa, which was maintained in RPMI-1640 plus 20% FCS (Katano H., pers. comm., 1999).

Activation of tumor cells and PBMNC

Tumor cells in suspension and PBMNC obtained in the second operation were cultured in anti-CD3 mAb-coated flasks in the presence of IL-2 (700 U/mL) and 10% human serum.[29] Virus induction of FDCS-Sa cells was performed by adding 5-iodo-2'-deoxyuridine (IdUrd, 50 μmol) to the culture medium for 72 h.[30]

Establishment of FDCS cell line (FDCS-Sa)

Tumor cells dispersed with collagenase (Wako Pure Chemicals) were initially cultured in DMEM plus 20% FCS with ECGF 10 and then serially replated to be established as an FDCS cell line, designated as FDCS-Sa, which was maintained in RPMI-1640 plus 20% FCS.

Collection of virus-like particles

Following centrifugation of the culture medium of tumor cells or PBMNC, cultured for 1 week with mAb in CD3-coated flasks, at 400 *g* for 20 min, the supernatant was further centrifuged on 5, 10, 20 and 30% sucrose gradient in PBS using an SW41 swing rotor (Beckman Coulter, Fullerton, CA, USA) at 2×10^5 *g* for 2 h. The precipitate in the interface between 20% and 30% sucrose was collected and fixed in 2.5% glutaraldehyde and processed for electron microscopy.

Reverse transcription–polymerase chain reaction using FFPE tissues

Total RNA was obtained from FFPE sections using the Pinpoint Slide RNA Isolation System IITM (Zymo Research, Orange, CA, USA) to detect viral RNA and also estrogen receptor (ER). The neoplastic tissue was manually dissected from FFPE sections using needles and analyzed using the Pinpoint Slide RNA Isolation System IITM in accordance with the manufacturer's protocol (Zymo Research). cDNA synthesis and polymerase chain reaction (PCR) were performed using a Takara RNA PCR kit at the Division of Surgical Pathology, Nippon Medical School, Tokyo, Japan. The primer pairs used for ER, CD21 as the inner control and β-actin as

Table 1 Antibodies used in immunohistochemistry

Antibody to	Clone	Source	Dilution	Antigenic retrieval	Tumor, first operation/secomd operation/FDCS-Sa
CD21	1F8	Dako, Glostrup, Denmark	×100	Proteinase K (Dako, Glostrup, Denmark)	++/++/++
Clusterin	7D1	Novocastra, Newcastle-upon-Tyne, UK	×500	Autoclave	++/NA/NA
CNA-42	M7157	Dako, Glostrup, Denmark	×100	LAB solution (Polysciences PA)	++/NA/NA
CD23	1B12	Novocastra, Newcastle-upon-Tyne, UK	×50	LAB solution (Polysciences PA)	+/+/NA
DRC-1	M0709	Dako, Glostrup, Denmark	×200	LAB solution (Polysciences PA)	+/NA/NA
S-100 α	SH-A1	Sigma, St Louis, MO, USA	×50	LAB solution (Polysciences PA)	+/NA/NA
CD123	7G3	Becton-Dickinson Japan	×400	Immunosaver (Nisshin EM, Tokyo, Japan)	–/NA/NA
CD137	BBK-2	Dako, Glostrup, Denmark	×100	LAB solution (Polysciences, Warrington, PA, USA)	+/NA/NA
Tyrosine hydroxylase	LNC1	Millipore, Billerica, MA, USA	×200	Immunosaver (Nisshin EM, Japan)	–/NA/NA
CD4	1F8	Novocastra, Newcastle-upon-Tyne, UK	×20	Immunosaver (Nisshin EM, Japan)	+/NA/NA
CD1a	O10	MBL, Woburn, MA, USA	×30	Immunosaver (Nisshin EM, Japan)	–/NA/NA
CD3	Rabbit polyclonal	Dako, Glostrup, Denmark	×500	Immunosaver (Nisshin EM, Japan)	–/NA/NA
CD20	L-26	Dako, Glostrup, Denmark	×10 000	Immunosaver (Nisshin EM, Japan)	–/NA/NA
CD57(Leu-7)	Leu-7(HNK-1)	Becton-Dickinson Japan	×100	Immunosaver (Nisshin EM, Japan)	–/NA/NA
CD68	KP-1	Dako, Glostrup, Denmark	×13 000	Immunosaver (Nisshin EM, Japan)	–/NA/NA
CD68	PGM-1	Dako, Glostrup, Denmark	×500	Immunosaver (Nisshin EM, Japan)	–/NA/NA
Keratin(Z6)	Z622	Dako, Glostrup, Denmark	×4 000	Immunosaver (Nisshin EM, Japan)	–/NA/NA
CAM5.2	kit(BD-349205)	Becton-Dickinson, San Jose, CA, USA		Immunosaver (Nisshin EM, Japan)	–/NA/NA
Chromogranin A	polyclonal	Dako, Glostrup, Denmark	×15 000	Immunosaver (Nisshin EM, Japan)	–/NA/NA
S-100-β	polyclonal	Dako, Glostrup, Denmark	×2 000	Immunosaver (Nisshin EM, Japan)	–/NA/NA
Synaptophysin	rabbit polyclonal	Dako, Glostrup, Denmark	×200	Immunosaver (Nisshin EM, Japan)	–/NA/NA
α-SMA	1A4	Dako, Glostrup, Denmark	×2 000	Immunosaver (Nisshin EM, Japan)	–/NA/NA
GFAP	polyclonal	Dako, Glostrup, Denmark	×1 000	Immunosaver (Nisshin EM, Japan)	–/NA/NA
ER-α	1D5	Abcam, Cambridge, MA, USA	×20	Immunosaver (Nisshin EM, Japan)	+/NA/NA
HMB45	HMB45	Dako, Glostrup, Denmark	×500	Immunosaver (Nisshin EM, Japan)	–/NA/NA
EMA	E29	Dako, Glostrup, Denmark	×1 500	Immunosaver (Nisshin EM, Japan)	–/NA/NA
EGFR	111.6	ThermoFisher Scientific, Waltham, MA, USA	×100	Immunosaver (Nisshin EM, Japan)	–/NA/NA
Placenta-ALP	polyclonal	Dako, Glostrup, Denmark	×1 600	Immunosaver (Nisshin EM, Japan)	–/NA/NA
HCG	polyclonal	Dako, Glostrup, Denmark	×400	Immunosaver (Nisshin EM, Japan)	–/NA/NA
C-kit	polyclonal	Dako, Glostrup, Denmark	×1 000	Immunosaver (Nisshin EM, Japan)	–/NA/NA
Ki-67	MIB-1	Dako, Glostrup, Denmark	×1 000	Immunosaver (Nisshin EM, Japan)	–/NA/NA

++, strongly positive; +, positive; –, negative; FDCS, follicular dendritic cell sarcoma; NA, data not available. Immunohistochemistry has not been done.

Table 2 Primer pair sequences

Oligonucleotide	Sequence
CD21 upper	5′-tacttctgcggttcagtgtc-3′
CD21 lower	5′-tgcccattgaggatgttag-3′
ER upper	5′- gcaatgactatgcttcaggctacc-3′
ER lower	5′- ctccctcctcttcggtcttttc-3′
β-Actin upper	5′-aagagaggcatcctcaccct-3′
β-Actin lower	5′-tacatggctggggtgttgaa-3′
HIV1 upper 1	5′-ggacatcaagcagcYatgcaaatg-3′
HIV1 upper 2	5′-ggacaccaRgcagctatgcaaatg-3′
HIV1 lower 1	5′-tgctatRtcacttccccttggttctct-3′
HIV1 lower 2	5′-tgctatatcacttcccctaggttccct-3′
HIV1 lower 4	5′-tgctatatcactcccccctaggttctct-3′
HIV1 probe	5′FAM-acHatcaatgaggaagctgcagaa-MGB-3′
HIV2 upper	5′-gcaggtagagcctgggtgttc-3′
HIV2 lower	5′-cttgcttctaaYtggcagctttatt-3′
HIV2 probe	5′-FAM-tgggcagaYggctccacgc-MGB-3′
HTLV1 upper	5′-cggatacccagtctacgtgttt-3′
HTLV2 upper	5′-cggataccccgtctacgtgttt-3′
HTLV1 lower	5′-gagagccgataacgcgtcca-3′
HTLV2 lower	5′-tcgagctgacaacgcgtcca-3′
HTLV probe	5′-FAM-Mtcacctgggaccccatcgatgga-MGB-3′
HBV upper	5′-gtggtggacttctctcaattttctag-3′
HBV lower	5′-ggacaMacgggcaacatacct-3′
HBV probe	5′-FAM-tgtctgcggcgtttt-MGB-3′
HCV upper	5′-gtctagccatggcgttagta-3′
HCV lower	5′-ctcgcaagcaccctatcaggcagt-3′
HCV probe	5′-FAM-tgcggaaccggttgagt-MGB-3′
B19 upper	5′-gggtttcaagcacaagYagtaaaaga-3′
B19 lower	5′-cggYaaacttccttgaaaatg-3′
B19 probe	5′-FAM-cagctgcccctgtgg-MGB-3′
GAPDH upper	5′-tgtgctcccactcctgatttc-3′
GAPDH lower	5′-cctagtcccagggctttgatt-3′
GAPDH probe	5′-FAM-aaaagagctaggaaggacaggcaacttggc-TAMRA-3′
EBV upper	5′-cggaagccctctggacttc-3′
EBV lower	5′-ccctgtttatccgatggaatg-3′
EBV probe	5′-FAM-tgtacacgcacgagaaatgcgcc-TAMRA-3′
VZV upper	5′-aacttttacatccagcctggcg-3′
VZV lower	5′-gaaaacccaaaccgttctcgag-3′
VZV probe	5′-FAM-tgtctttcacggaggcaaacacgt-TAMRA-3′
HSV upper	5′-cgcatcaagaccacctcctc-3′
HSV lower	5′-gctcgcaccacgcga-3′
HSV1 probe	5′-JOE-tggcaacgcggcccaac-TAMRA-3′
HSV2 probe	5′-FAM-cggcgatgcgccccag-TAMRA-3′
CMV upper	5′-catgaaggtctttgcccagtac-3′
CMV lower	5′-ggccaaagtgtaggctacaatag-3′
CMV probe	5′-FAM-tggcccgtaggtcatccacactagg-TAMRA-3′
HHV6 upper	5′-gacaatcacatgcctggataatg-3′
HHV6 lower	5′-tgtaagcgtgtggtaatgtactaa-3′
HHV6 probe	5′-FAM-agcagctggctaaaagtgctgtgc-TAMRA-3′
HHV7 upper	5′-cggaagtcactggagtaatgacaa-3′
HHV7 lower	5′-ccaatccttccgaaaccgat-3′
HHV7 probe	5′-FAM-ctcgcagattgcttgttggccatg-TAMRA-3′

FAM, JOE, MGB, TAMRA, dyes to determine locations.
H, M, R, and M, mixed bases of A/T/C, A/C, A/G, and C/T, respectively.
ER, estrogen receptor; GAPDH, glyceraldehyde 3-phosphate dehydrogenase; HHV, human herpesvirus, HSV, Herpese simplex virus; HTLV, human T-cell leukemia virus; VZV, Varicella zoster virus.

the positive control are listed in Table 2. PCR was carried out in a Takara PCR thermal cycler MP (Takara, Tokyo, Japan) for 2 min at 94°C, followed by 35 cycles, each consisting of 30 s at 94°C, 30 s at 60°C, and 2 min at 72°C. The authenticity of the PCR product was confirmed on direct sequencing. Total RNA not subjected to reverse transcription was used as the negative control.

Virology

To further examine negativity for the antibody to EBV determined by laboratory examination, multiplex real-time PCR was performed to detect other viruses in biopsied tumor tissues and peripheral blood specimens as previously described at the Department of Comprehensive Pathology, and Department of Virology, Division of Medical Science, Medical Research Institute, Tokyo Medical and Dental University, Tokyo, Japan.[31] Genomes for Herpes simplex virus (HSV)1, HSV2, Varicella zoster virus (VZV), CMV, human herpesvirus (HHV)6, BK virus (BKV), JC virus (JCV), Parvo virus B19, EBV, HHV-7, HHV-8, HBV, HIV-1, HIV-2, human T-cell leukemia virus (HTLV)-1, HTLV-2, and HCV were determined in fresh tissues of the recurrent tumor. The samples were tested for DNA of the aforementioned viruses as well as the cDNAs of HIV-1, HIV-2, HTLV-1, HTLV-2, and HCV on multiplex PCR screening test at the Center for Cell Therapy of Tokyo Medical and Dental University. cDNA of FDCS-Sa was also analyzed for interferon (INF)-α INF-β, and INF-γ on multiplex PCR screening.[31]

RESULTS

Cytology

Papanicolaou-stained direct smears of the FNA tumor specimens indicated a background of small lymphocytes and a moderate number of monomorphic atypical cells with a vesicular nucleus showing a delicate nuclear membrane, fine vesicular chromatin and small distinct nucleoli in semicohesive clusters (Fig. 1a). The atypical cells were threefold larger than the small lymphocytes, and had an abundant granular cytoplasm and indistinct cell border. Giant cells and abnormal cells with bizarre nuclei were not observed.

The tumor cells in cell block sections were negative for CAM5.2, S-100-β, PGM-1(CD68), leukocyte common antigen, and myeloperoxydase on immunohistochemistry.

Metastatic carcinoma, oncocytic carcinoma of salivary gland, Langerhans cell histiocytosis, malignant granular cell tumor, malignant lymphoma, and leukemia were ruled out and we were not able to make a definitive diagnosis in the initial cytological assessment.

Histology and immunochemistry

The specimens obtained from the first operation showed sheets of pale eosinophilic elongated cells with fine nucle-

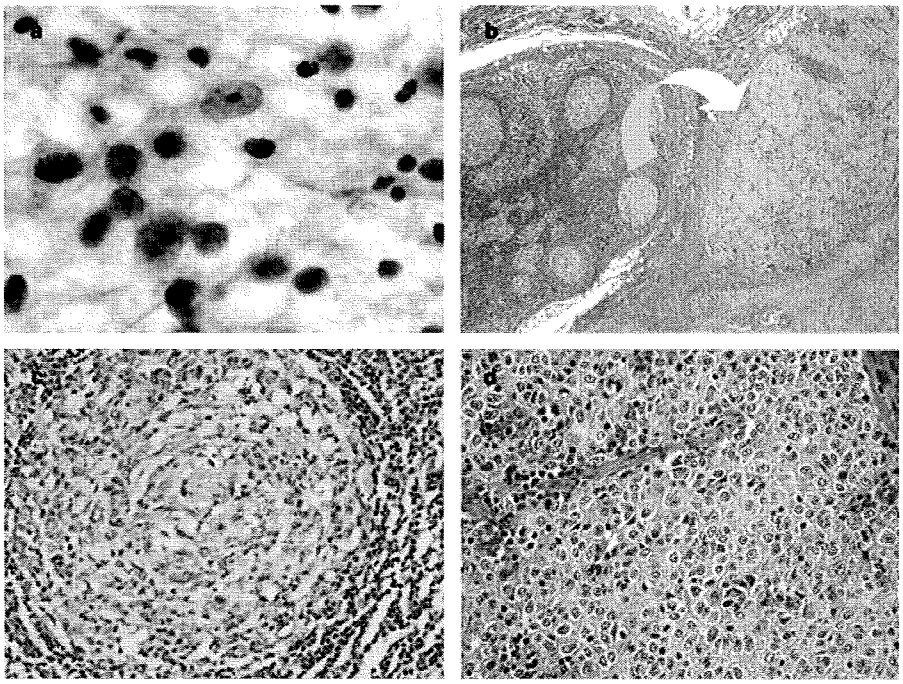

Figure 1 Cytology and histology. (**a**) Needle-biopsied smeared specimen of the cervical tumor showing enlarged, granular mesenchymal cells with euchromatic nuclei and small lymphocytes admixed (Papanicolaou-stain). (**b**) The tumor mass is well delineated with fibrous connective tissue and incompletely divided into nodules by fine fibrovascular septa. The lymph nodes neighboring the tumor mass contained some distorted germinal centers (HE). (**c**) The distorted GC displays a proliferation of dysplastic follicular dendritic cells, irregularly distributed, accompanying angiosclerotic change and pyknotic lymphoid cells. No light and dark zone is discernible. No tingible body macrophages (HE). (**d**) The cervical tumor shows a solid proliferation of pale acidophilic, plump ovoid cells with single to several nucleolated euchromatic nuclei, accompanying hypervascularization and lymphocyte infiltration in varying degrees (HE).

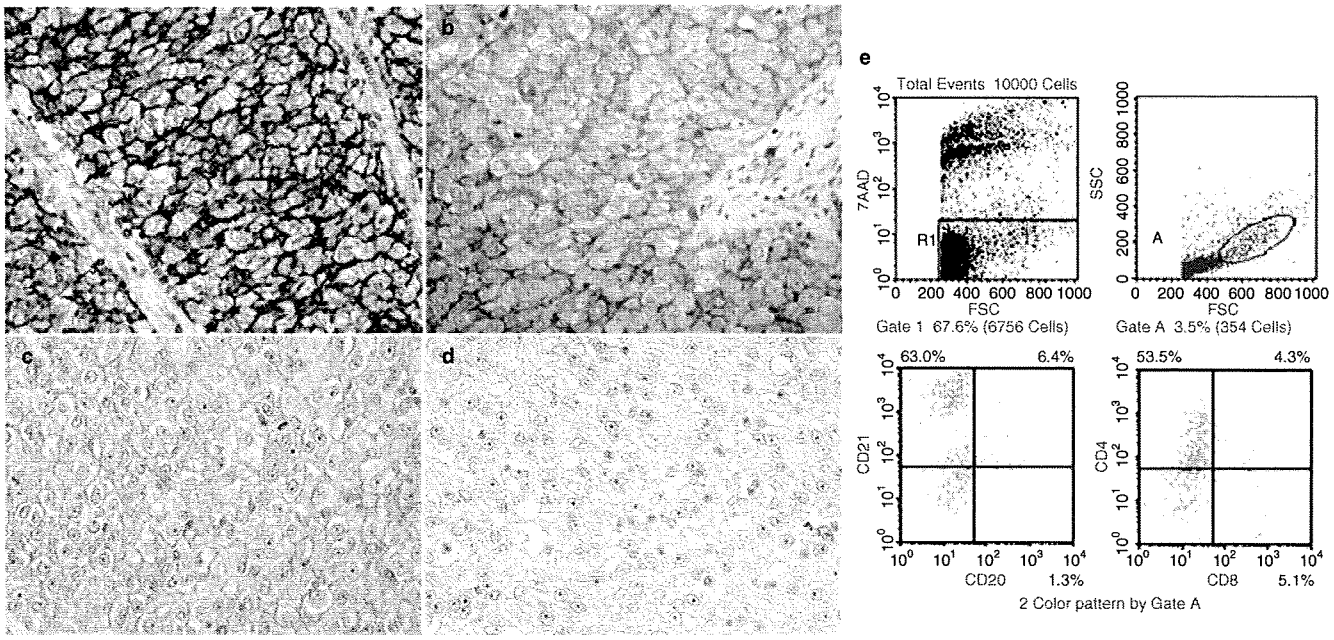

Figure 2 Immunostaining and flow cytometry. Immunohistochemistry is strongly positive for (**a**) CD21 and (**b**) clusterin, and weakly positive for (**c**) CD4 and (**d**) estrogen receptor-α in tumor cells. (**e**) On flow cytometry, enlarged cells or tumor cells are positive for CD21 (69.4%, gate A), and CD4 (57.8%, gate A), and negative for CD8 (9.4%, gate A). FSC, forward scatter.

olated vesicular nuclei and indistinct cell border. Atypical mitosis was observed in 7–8/10 high-power fields. Thin fibrous and vascular-rich septa formed some compartments of the tumor cells. Small lymphocytes were scattered in the compartment and septae (Fig. 1d). The tumor was well encapsulated without stromal invasion. Lymph nodes neighboring the tumor showed some distorted GC containing dysplastic FDC and gradual expansion of tumor cells to surrounding tissues via the paracortical and medullary regions (Fig. 1b). Some neighboring lymph nodes showed no changes of FDC in GC. A higher magnification view of distorted GC showed scattered atypical FDC, with hyperchromatic and nucleolated vesicular nuclei accompanying loss of polarity. They were often arranged in a whorled pattern

around the artery in GC. Pyknotic lymphoid cells were intermingled. No distinction of the light zone and dark zone nor tingible body macrophages were seen (Fig. 1c).

Tumor cells were consistently positive for CD21 and clusterin, variably positive for CNA.42, and weakly positive for DRC-1, CD23, CD137 and S-100-α (Table 1; Fig. 2a–d). Osteopontin, as well as GM1 ganglioside, was also confirmed to be positive not only in tumor cells en bloc but also in the established FDCS-Sa cell line.[32,33] Interestingly, CD4 and ER, particularly those of the alpha subtype (ER-α) were diffusely positive with mild intensity in the tumor cells (Fig. 2a–d).

The ki-67 index of the tumor was approximately 20%, suggesting intermediate–high-grade malignancy, whereas some tumor tissues were exposed in the sinus or lymph vessels. A diagnosis of FDCS arising from the left cervical lymph nodes was made.

The recurrent tumor extirpated 19 months after the first operation had spindle-shaped, slightly pleomorphic tumor cells arranged in a whorl-like pattern with an increased number of mitosis and ki-67 index, approximately 40%, suggesting a higher grade of malignancy than the tumor operated on previously.

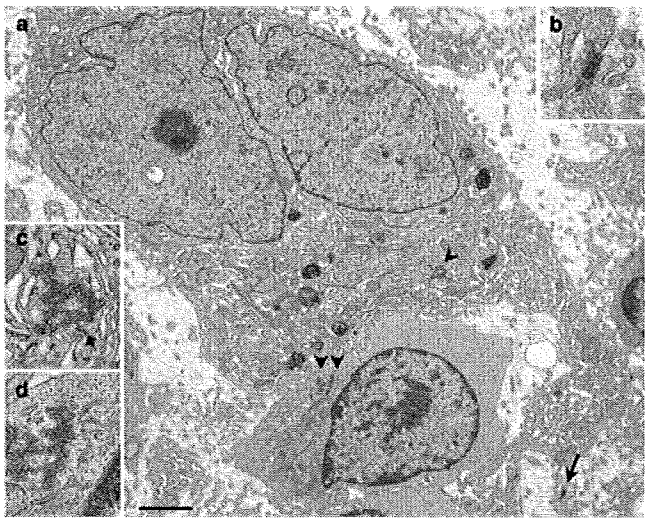

Figure 3 Electron microscopy of tumor. (**a**) The tumor cells are elongated with nucleolated, euchromatic nuclei, abundant meandering rough endoplasmic reticulum (rER), and filiform cytoplasmic extensions (bar, 2 μm). Arrow, desmosome-like junction; single arrowhead, microtubuloreticular structures (MTRS) in a tumor cell; double arrowhead, MTRS in the associated lymphocyte. (**b**) Desmosome-like junctions characterizing intercellular connections of follicular dendritic cell sarcoma. (**c**) Microtubuloreticular structures are often encountered in the cytoplasm not only in tumor cells, but (**d**) also in infiltrating lymphoid cells.

Reverse transcription–polymerase chain reaction

Reverse transcription–PCR (RT-PCR) of cDNA obtained from RNA of specimens manually dissected from FFPE tumors with a needle indicated the presence of ER-α/β, CD21, as the marker of the tumor, and β-actin as the internal marker (data not shown).

All tests for any conventional infectious and oncogenic viruses were negative. These included serum antibodies for EBV, serum real-time PCR of EBER transcripts and multiplex real-time PCR screening of HHV-8, BKV, JCV, ParvoB19, HBV, HCV, HGV, HIV-1, HIV-2, HTLV-1, and HTLV-2 using isolated cDNA from tumor cells and cultured PBMNC (data not shown).

Electron microscopy

The tumor cells obtained in the first extirpation were large and atypical, with a complex of long cytoplasmic processes joined by desmosome-like junctions (Fig. 3a,b). The nuclei were large and irregularly outlined, containing dispersed chromatin and prominent nucleoli. The cytoplasm contained a well-developed Golgi apparatus, abundant rough endoplasmic reticulum (rER), and rich polyribosomes, and scattered lysosomal vesicles. Pinocytic vesicles focally delineated the cytoplasmic membrane, and multivesicular bodies were also observed to be closely associated with pinocytic vesicles. MTRS, electron-dense reticular packages of fine tubular structures, were found in the cytoplasm of some tumor cells as well as infiltrating lymphocytes at similar frequencies (Fig. 3a,c,d).

In the recurrent tumor specimen the tumor cells were ultrastructurally similar to cells from the tumor removed in the first operation. MTRS were observed in both tumor cells and lymphocytes. We noted that MTRS often occurred in connection with the membrane of rER, particularly in the recurrent tumor (Fig. 4a–c). In some cells, ring-shaped cisternae including loose tubuloreticular structures or tubular confronting cisternae were also observed.[34]

Atypical large mononuclear spindle-shaped cells were found in the PBMNC cytospun specimen. They clustered in culture, and ultrastructurally they had desmosome-like junctions between abutting atypical spindle-cells but no MTRS.

Collagenase-dispersed cells of the recurrent tumor cultured in anti-CD3 mAb-coated flask with IL-2 (700 U/L), 3 days after culture, had small vacuoles in the cytoplasm after cytospinning and Giemsa staining. On electron microscopy they were intracytoplasmic cysts, varying from 1 to 3 μm in diameter, filled with fine small round electron-lucent vesicles (sELV), 30–40 nm in diameter such as seen in HIV-1 infection (Fig. 4d,e).[35] Such vesicles were also observed in the tumor cells. Twisted microstrands or loosened MTRS were residually confirmed in the margin of the cysts (Fig. 4e, arrow).

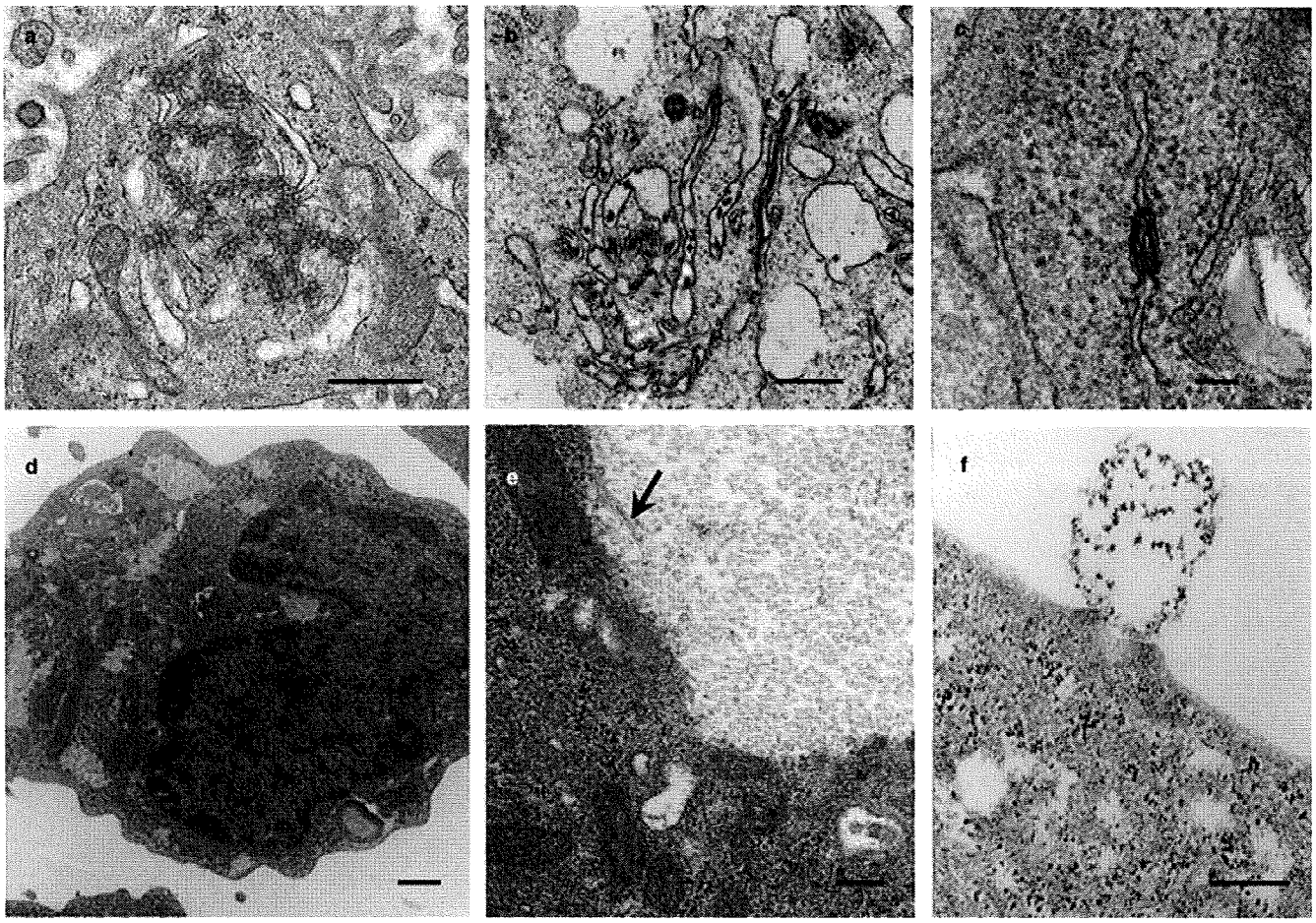

Figure 4 Electron microscopy of microtubuloreticular structures (MTRS) and intracytoplasmic cysts in cultured cells. (**a–c**) Profiles of MTRS in tumor cells and admixed lymphocytes in the recurrent tumor. In addition to typical (**a**) MTRS, (**b**) rough endoplasmic reticulum (rER) with threadlike structures and (**c**) knitted nodules of rER are observed in tumor cells and lymphocytes. These findings suggest that the MTRS were derived from rER. (**d–f**) Two types of vesicle in cytoplasm in lymphoid cells and tumor cells, when cultured in the presence of anti-CD3 antibody and interleukin (IL)-2. (**d**) Some tumor cells and lymphocytes suspended and cytospun show intracytoplasmic vacuoles of varying sizes on light microscopy. On electron microscopy the cysts were filled with small electron-lucent vesicles (sELV), approximately 30–40 nm in diameter. (**e**) Some tubular structures are also detected in the cyst, which are possibly residual MTRS. (**f**) Furthermore, tumor cells occasionally show another type of intracytoplasmic cyst, which is barrel-shaped and contains a mixture of electron-lucent and -dense granules (mLDG), approximately 10–20 nm in diameter. Some cysts are bursting and releasing mLDG, approximately 5 nm in diameter, into the media. Bars: a,b,d,f, 500 nm; c,e, 100 nm.

Although the culture in anti-CD3 mAb-coated flask with IL-2 (700 U/L) showed rapid proliferation of lymphoid cells, FDCS cells gradually became atrophic (Fig. 5a). On the seventh day of culture, electron-dense VLP were recognized on the outer cell membrane and occasionally in the cytoplasm both in tumor cells and lymphoid cells (Fig. 5b,c). VLP were electron-dense granulated or conglomerated round structures, approximately 100 nm in diameter. The core of VLP consists of electron-dense fine granules approximately 30–40 nm in diameter. Similar VLP with some corona were also found in the nucleus and cytoplasm of distorted tumor cells (Fig. 5d). Some VLP were budding from an electron-dense elevated cytoplasmic membrane from lymphoid cells.

The cell line of FDC (Fig. 6a,b), established and designated as FDCS-Sa, consisted of spindle-shaped cells highly resembling FDC-like cells (FDCLC48 cited previously by Taruishi *et al.*[6]) obtained from tonsils of a patient with chronic tonsillitis. They extend several elongated ramifying processes, lined disconnectedly by spinelike spiculae as well as desmosome-like junctions, to form networks. They are abundant in organellae as found in the primary culture of the tumor cells. Barrel-shaped cysts, approximately 2 μm long and 1 μm wide, were found in the periphery of the cytoplasm, containing a mixture of electron-dense and -lucent granules, 10–20 nm in diameter, tentatively designated as a mixture of electron-lucent and -dense granules (mLDG). In some cultures the barrel-shaped cysts containing mLDG inversely

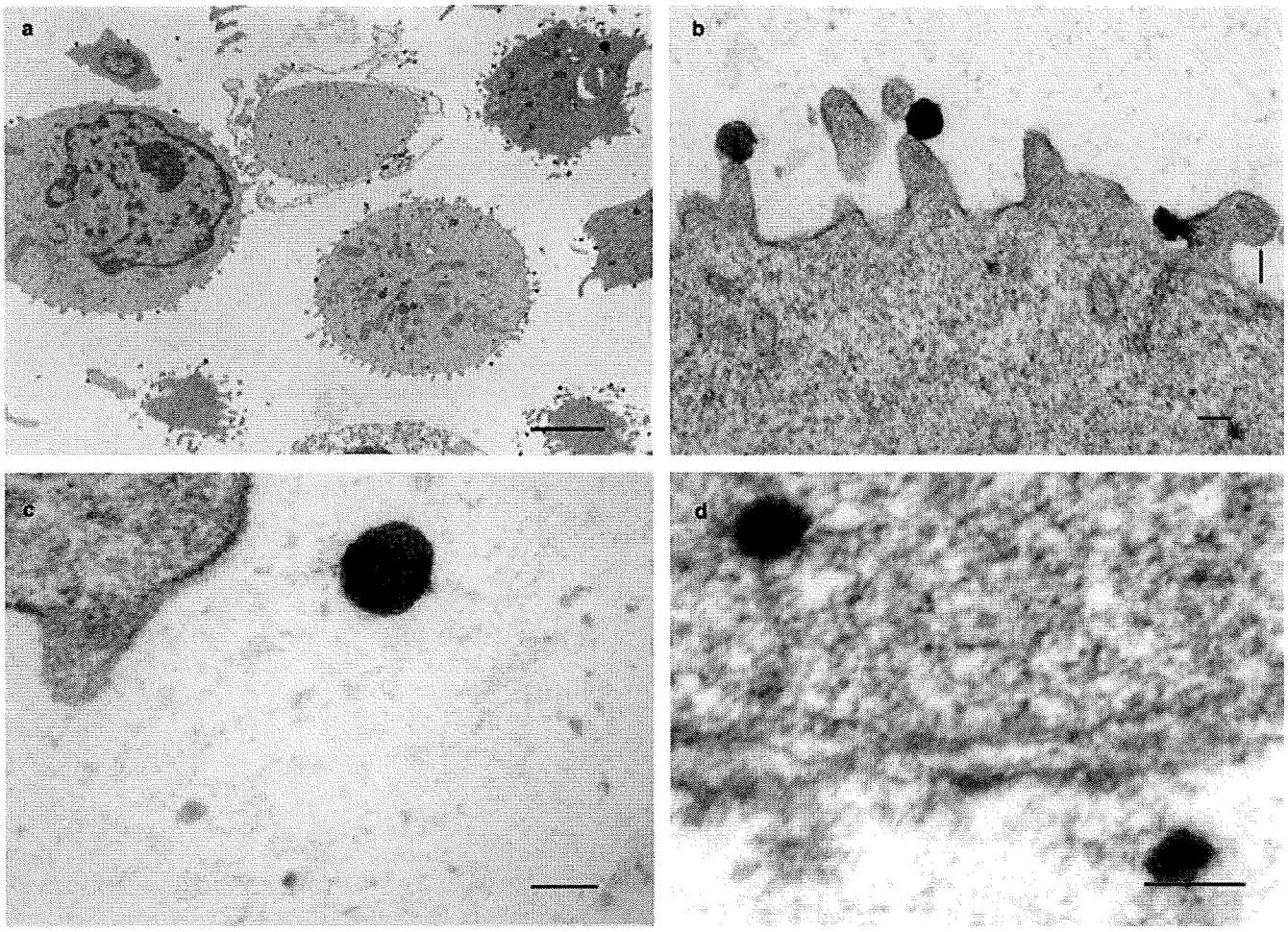

Figure 5 Electron microscopy of cultured follicular dendritic cell sarcoma (FDCS)-Sa in anti-CD3 mAb-coated flasks with interleukin (IL)-2. (**a–c**) Cells dispersed from the recurrent tumor and cultured in anti-CD3 mAb-coated flasks with IL-2 for 7 days show electron-dense virus-like particles (VLP), approximately 100 nm in diameter, budding off from cytoplasmic extensions of lymphoid cells. (**d**) Similar particles are also found in the nucleus of degenerated tumor cells. Note that the VLP are electron-dense and glomerular in shape with a wavy circumference. Bars: a, 500 μm; b–d, 100 nm.

bulged out of the cytoplasmic membrane and released mLDG in the medium (Fig. 4f).

The mLDG were different from sELV observed in cysts appearing in the early stage of anti-CD3 and IL-2 mAb-stimulated tumor cells and lymphoid cells. These sELV and mLDG seem different from VLP but instead appeared to be some virus infection-associating structure. sELV are well described also in HIV-1 infection.[36]

Instead of anti-CD3 mAb and IL-2, we stimulated FDCS-Sa with IdUrd, another virus replication agent, to induce VLP replication. Three days later, budding off florid electron-dense VLP in the periphery of the cytoplasm and the release of these VLP to medium were observed (Fig. 7a,b). The cytoplasmic membrane of FDCS-Sa was coated with an extracellular band, 500–1000 nm in width, of an amorphous moderately electron-dense matrix. In the coating matrix, VLP budded off from the cytoplasmic membrane and then dispersed through the coat towards the free medium. In these VLP-producing phases it was difficult to find MTRS, but smaller cysts containing mLDG or sELV were occasionally found.

VLP were collected by ultracentrifugation from the supernatant of the medium in which tumor cells or PBMNC were cultured with anti-CD3 and -IL-2 mAb, and FDCS-Sa cells were cultured with IdUrd. On electron microscopy these VLP were round and sea-urchin-shaped, approximately 100 nm in diameter, with an envelope composed of electron-dense thorns and an electron-lucent core (Fig. 7c,d). In some photos of the VLP the core contained a package tiled by electron-lucent hexagonal units with a diameter of 10–20 nm. At higher magnification some hexagonal units were outlined with electron-lucent 5 nm-sized beads and had an electron dense rod or base of the spiculae in the envelope.

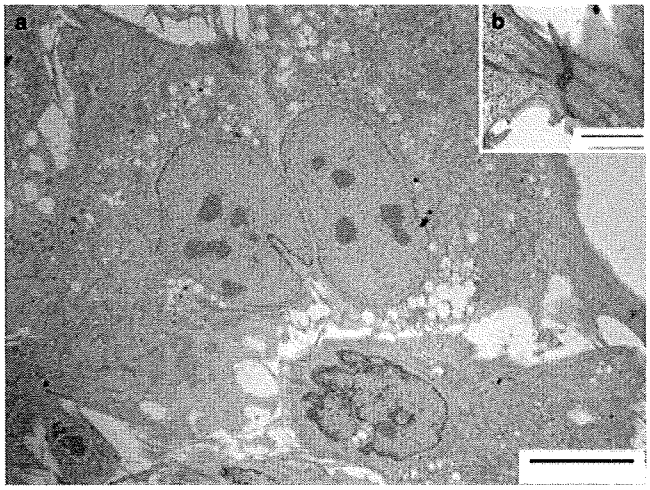

Figure 6 Electron microscopy of cell line established from recurrent tumor (follicular dendritic cell sarcoma (FDCS)-Sa). (**a**) FDCS-Sa with meandering rough endoplasmic reticulum (rER) and vacuoles as well as cytoplasmic extensions. Neither microtubuloreticular structures (MTRS) nor virus-like particles (VLP) were found in the cytoplasm, whereas such vesicles as shown in Fig. 4(e,f) are detected. Bar, 10 μm. (**b**) Desmosome-like junctions are also found in the opposing cytoplasmic extensions.

DISCUSSION

Neoplasm of FDC was first proposed by Lennert *et al.* in 1978 and described by Monda *et al.* in 1986 as FDCS.[37,38] Different from spindle-shaped cell sarcomas, FDCS is known to have at least intermediate-grade malignancy and is diagnosed on the basis of immunohistochemistry and electron microscopy hallmarks including CD21-related antigens and desmosome-like junctions. The tumor tissue is compartmentalized by fibrous septae rich in vasculature. Lymphoid cell infiltration also characterizes FDCS. Reviewing the literature, the number of FDCS diagnoses has recently increased, and some malignant spindle-shaped cell tumors of unknown origin have been occasionally classified into FDCS. Some cases involved typical desmosomes with thick bundles of tonofilaments rather than desmosome-like junctions, indicating a misdiagnosis of spindle-shaped cell cancer. In addition, however, to hallmarks of FDCS, the present case is highly representative, demonstrating on microscopy its origin from atypical FDC in the GC of lymph nodes and its expansion to clusters of FDCS cells in the extranodal mass, supporting the present interpretation that FDC in GC give rise to FDCS.

Among the hundreds of FDCS cases hereto reported, the present case is peculiar in terms of the presence of MTRS in tumor cells and lymphoid cells, suggesting viral infection, and in terms of actual evidence of VLP production of tumor cells when cultured with virus-replication-promoting agents.

MTRS were first described by Chandra in lymphoblasts of a leukocyte culture,[39,40] and have most frequently been described in endothelial cells and peripheral blood lymphocytes of active systemic lupus erythematosus and miscellaneous viral infections and neoplastic conditions: systemic endothelia and circulating lymphocytes in HIV infection,[35,36,41,42] Herpes simplex, and human eastern equine encephalitis, and children with severe combined immunodeficiency diseases.[43,44] These structures were also noticed in two B-cell lines of infectious mononucleosis and tumor cells of Burkitt-type lymphoma,[45,46] germinoma, and interdigitating cell sarcoma.[47,48] These reports duly suggest an intimate relationship between MTRS and viral infection. In the present case viral infection cannot be excluded, although wide-ranging clinico-laboratory analysis of viral infection on RT-PCR and/or real-time PCR found no evidence for a broad spectrum of viruses including oncogenic viruses. On ultrastructure, MTRS in the present case were occasionally found to be in continuity with some dilated rER-containing vesicles, crystals, and threadlike structures with periodicity (Fig. 4b,c). Neither VLP nor budding forms, however, were observed in non-stimulated MTRS-bearing tumor cells and lymphoid cells. Subsequently, we examined the relationship between MTRS and FDCS. No MTRS have been observed in FDCS, at least in the literature, including 30 case reports of FDCS involving electron microscopy, and there have been no reports on the involvement of oncogenic viral infection in tumor genesis of FDCS (using PubMed (NLM) and MEDLINE (ICHU) search). EBV infection has been noted in a few FDCS in cases of EBV infection: one out of six Japanese patients and one out of 35 patients in three reviews using RT-PCR and/or ISH-EBER.[18,24,49,50] Even in EBV-positive cases, no MTRS were observed. In contrast, Hiraoka *et al.* demonstrated MTRS in leukemic cells and PBMNC in a case of hairy cell leukemia after *in vitro* and *in vivo* administration of IFN-α.[51] Furthermore, a similar induction of MTRS is also documented by others.[52–54] MTRS are reported to be induced by IFN-α or IFN-β but not by IFN-γ.[55,56]

These reports indicate that MTRS are feasibly induced in tumor cells and PBMNC by IFN-α administered or internally induced by some viral infection. Although plasmacytoid dendritic cell is well known to produce IFN-α, MTRS have never been reported in the neoplasm of such cells. Of course, the present case did not arise from plasmacytoid DC or CD4+/CD56+/IFN-α-producing DC, but from FDC.[57] There has been no report on IFN-α production in FDC or FDCS as noted here. RT-PCR of cDNA in FDCS-Sa indicated expression of IFN-β and IFN-γ but not that of IFN-α (data not shown). In this case, because there was no therapeutic administration of IFN-α, there remains the possibility of some virus infection as the cause of MTRS formation. Despite the multiplex PCR qualitative analysis of various pathogenic DNA and RNA viruses performed at the Center of Cell Therapy showing the absence of such infection, there remains the possibility of some unusual unknown or endog-